Investments in photoreceptors compete with investments in optics to determine eye design

Francisco J H Heras[1] and Simon B Laughlin*[1]

[1]Department of Zoology, University of Cambridge, U.K.

Abstract

When an animal invests space, materials and energy in an eye to meet behavioural needs, the eye's optics and photoreceptor array compete for these resources to improve the eye's performance. To discover how this competition influences eye design, we introduce a new and superior measure of cost, specific volume in $\mu m^3\,sr^{-1}$, that depends on the dimensions of the eye's components, applies to both optics and photoreceptor array, accounts for space, materials and energy (including photoreceptors' high metabolic rates), and links investments to an eye's performance via optical, physiological and geometrical constraints. Specific volume enables us to construct a performance surface across the morphospace of an eye of given type and total cost by modelling all of its configurations and determining each model's information capacity. We model three eye types, neural superposition and fused-rhabdom apposition compound eyes and a simple (camera type) eye, across a 10^5-fold range of total cost. Performance surfaces are flat-topped, therefore the optimum configuration lies in a broad high-efficiency zone within which eyes adapted for specific tasks loose <5% of information. This robust region will increase adaptability by reducing loss of function. Comparing optimised models: simple eye information capacity increases as $(\text{total cost})^{0.8}$ and $(\text{total cost})^{0.55}$ in apposition eyesm and simple eyes are x10 to x100 more efficient than apposition eyes of the same total cost. In both eye types 30%- 80% of total cost is invested in photoreceptor arrays, optimum photoreceptor length increases with total cost and is reduced by photoreceptor energy consumption. Simple eyes' photoreceptors are much shorter than apposition eyes' and their length more sensitive to energy consumption. We analyse published data that cover the same range of total specific volumes. The apposition eyes of fast-flying diurnal insects follow three trends predicted by our models: photoreceptor arrays are allocated 40% - 80% of total specific volume, spatial resolution and photoreceptor length increase with increasing specific volume, and apposition photoreceptors are much longer than simple. We conclude that photoreceptor costs are considerable and often exceed optical costs. Thus, competition between optics and photoreceptors for resources helps determine eye design, photoreceptor energy cost plays a major role in determining an eye's efficiency and design, and matching investments in optics and photoreceptors to improve efficiency is a design principle. Our new methodology can be developed to view the adaptive radiation of eyes through a cost-benefit lens.

*Corresponding author sl104@cam.ac.uk

Introduction

The design of eyes has long fascinated biologists with its variations, innovations, numerous adaptations of form to function, and insights into the evolution of organs, both rudimentary and perfectly contrived (Darwin, 1859; Land & Fernald, 1992; Nilsson & Land, 2012; Oakley & Speiser, 2015; Walls, 1942). We address a question of eye design that has not been considered before, but is familiar to people who construct imaging systems on tight budgets. How should the resources invested in an eye be divided between an eye's two major components, the optical system that forms images and the photoreceptor array that captures images?

The benefits of enlarging the dioptric apparatus and the photoreceptor array are well understood, consequently numerous studies relate measures of eye morphology (radius, width, length, lens diameter, pupil area, and photoreceptor length) to optical, geometrical and physiological constraints on performance to show how morphology adapts an eye to lifestyle and habitat (Barlow, 1952; Kirschfeld, 1976; Labhart & Nilsson, 1995; Land, 1981; Land, 1997; Nilsson & Land, 2012; Niven et al., 2007; Snyder, 1979; K. N. Thomas et al., 2020). However, the fact that an eye's performance depends on two systems that effectively compete for the resources invested in an eye, the dioptric apparatus and the photoreceptor array, is rarely considered (Kirschfeld, 1976; Kröger & Biehlmaier, 2009). We investigate how trade-offs between dioptrics and photoreceptor array determine an eye's performance and efficiency by developing a new cost-benefit approach, which uses measures of eye morphology to calculate costs, and relates these measures to optical, geometrical and physiological constraints to calculate benefits.

We consider three basic eye types, two types of apposition compound eye, neural superposition and fused rhabdom, and a simple eye (Figure 1). We establish and road test our cost-benefit approach using apposition compound eyes because they offer a unique combination of advantages. The optical and physiological constraints are well documented, their effects on performance are measured and modelled, (Hardie & Postma, 2008; Heras & Laughlin, 2017; Howard et al., 1987; Snyder, 1979; Song et al., 2012; Stavenga, 2004b) and their influence on eye design is well established. For example, the compound eyes of housefly, praying mantis, dragonfly and robber fly have foveas for detecting, locating and catching flying mates or prey. Here the facet lens are enlarged to reduce the diffraction limit to optical resolving power, the ommatidia are more densely packed to increase angular resolution, and photoreceptors are elongated to increase signal to noise ratio by transducing more photons (B. G. Burton & Laughlin, 2003; Hardie, 1985; Labhart & Nilsson, 1995; Rossel, 1979; Wardill et al., 2017). In addition, there are clear indications that photoreceptors are costly and investments in optics and photoreceptors are matched. Apposition eyes' photoreceptor arrays obviously fill a substantial fraction of eye volume because photoreceptors construct long photoreceptive waveguides (rhabdomeres, rhabdoms), substantial photoreceptor energy costs increase with rhabdomere length (Niven et al., 2007), and there is a precise, fine scale covariation of acuity and photoreceptor length, measured in two apposition eyes (Labhart & Nilsson, 1995; Rossel, 1979) and obvious in many others (e.g. Figure 1b).

Our new cost-benefit approach establishes that photoreceptor cost is a major factor in eye design that influences optics by competing for the resources invested in

an eye. Consequently matching investments in optics and photoreceptors to improve efficiency is a principle of eye design. This principle can explain why apposition eyes have longer photoreceptors than simple eyes and photoreceptor length increases with spatial acuity in apposition and simple eyes. We suggest that our approach can advance our understanding of visual ecology by costing the benefits of the adaptions observed in eyes (Cronin et al., 2014; Nilsson & Land, 2012). Moreover, because the allocation of resources to optics and photoreceptors both promotes cost-effectiveness, and depends upon developmental and physiological mechanisms (Casares & McGregor, 2021; Niven & Laughlin, 2008), our cost-benefit approach may well contribute to our understanding of how and why eyes evolve (Nilsson & Pelger, 1994).

Symbols used in the Results and the Discussion

symbol	description	units
D	lens diameter	µm
f	lens focal length, in air	µm
f'	focal distance	µm
F	F-number	
d_{rh}	diameter of rhabdom (fused-rhabdom eye) or rhabdomere (NS eye)	µm
$\Delta\phi$	interommatidial or interreceptor angle	rad (Equations) deg (Figures)
R	radius of eye or locally spherical eye region	µm
p	eye parameter	
L	length of rhabdom or rhabdomere, also depth of photoreceptor array	µm
λ	wavelength of light	nm
η_i	refractive index of eye's internal medium	
$\Delta\rho_l$	half width of lens point-spread-function	rad
$\Delta\rho_{rh}$	half-width of rhabdom(ere) acceptance angle	rad
$\Delta\rho_{ph}$	half-width of photoreceptor acceptance angle	rad
V_o	volume of optics	$\mu m^3\,sr^{-1}$
$V_p h$	volume of photoreceptor array	$\mu m^3\,sr^{-1}$
V_{tot}	total eye volume	$\mu m^3\,sr^{-1}$
C_o	cost of optics	$\mu m^3\,sr^{-1}$
C_{ph}	costs of photoreceptor array	$\mu m^3\,sr^{-1}$
C_{tot}	total cost of eye	$\mu m^3\,sr^{-1}$
S_E	photoreceptor energy surcharge	$\mu m^3\,sr^{-1}$
K_E	photoreceptor energy tariff	$\mu m^3\,sr^{-1}$ per microvillus
N_{vil}	number of microvilli	
ν	number of microvilli per unit length of rhabdom or rhabdomere	μm^{-1}
ψ	transduction rate	
SNR_{ph}	photoreceptor signal to noise ratio	per unit contrast
H	spatio-temporal information capacity	bits sr^{-1} s^{-1}

Results

We start with the neural superposition (NS) eyes of flies. This type of apposition compound eye provides both the detailed analyses of optical and physiological constraints required to develop a model that relates investments in optics and photoreceptor arrays to performance, and the published data on dioptrics and photoreceptor arrays required to test our model. Moreover, because fly NS eyes vary in size between species while retaining similar structure and function we simplify our study by developing and using a generic fly NS model. We then model and examine fused rhabdom apposition eyes to identify general principles of apposition eye design. Finally we model a simple (camera) eye to demonstrate that changing eye type changes the distribution of costs. In all three types, we consider diurnal eyes operating in daylight when the number of available photons is not limiting. Although this restriction eliminates the many ways in which eyes are designed to operate efficiently at lower light levels (Nilsson & Land, 2012), it makes it easier to establish points of principle by reducing the numbers of variables in our models.

Calculating the benefits and costs of investing in optics

In daylight, when the number of available photons is not limiting, investments in optics buy increased optical contrast and spatial resolving power by reducing optical and geometrical constraints, as follows. An apposition eye forms and captures images with an array of ommatidia (Figure 1). Each ommatidium uses a facet lens of diameter, D, and focal length (in air), f, to focus light onto the entrance aperture of photoreceptive waveguides, a single fused rhabdom or several rhabdomeres (Figure 1) of diameter d_{rh} . Increasing D sharpens a photoreceptor's angular sensitivity by reducing the blur produced by the Airy disk diffraction pattern, whose half-width $\Delta\rho_L = \lambda/D$ radians, where λ is the wavelength of light, taken to be 500 nm. Increasing f and reducing d_{rh} also sharpen angular sensitivity by reducing the angular subtense of the photoreceptor entrance aperture, d_{rh}/f. Sharpening angular sensitivity has two benefits: it increases spatial resolving power and increases image contrast.

We calculate the effects of D, d_{rh} and f on the half-width of a fly photoreceptor's angular sensitivity, $\Delta\rho$, using two formulae, Snyder's simplification, his Convolution of Gaussians (CoG) $\Delta\rho^2 = \Delta\rho_L^2 + \Delta\rho_{rh}^2$, where $\Delta\rho_L = \lambda/D$ and $\Delta\rho_{rh} = d_{rh}/f$; and Stavenga's better approximation, $\Delta\rho = 1.26\Delta\rho_L$, obtained using a comprehensive wave-optics model (WOM) of flies' NS eyes operating in bright light (see Methods for more details). For CoG we fix $d_{rh} = 1.9$ µm because this value is typical of fly R1-6 (Hardie, 1985). CoG provides a lower bound to optical resolving power and WOM a more efficient upper bound that, in bright light, makes better use of investments in optics by operating closer to the diffraction limit.

The benefits of investing in optics come at a cost: increasing D and lengthening f to reduce $\Delta\rho$ expands the volume of the dioptric apparatus, V_o, which in apposition eyes is easily calculated from eye geometry (Figure 1e). D and $\Delta\phi$ define the radius $R = D/\Delta\phi$ of a locally spherical eye region, in which the dioptric apparatus (lens, cone and screening pigment) is a shell of thickness f', the focal distance from lens front surface to focal plane. Thus

$$V_o = \frac{1}{3}[R^3 - (R - f')^3] \ \mu\text{m}^3\,\text{sr}^{-1} \tag{1}$$

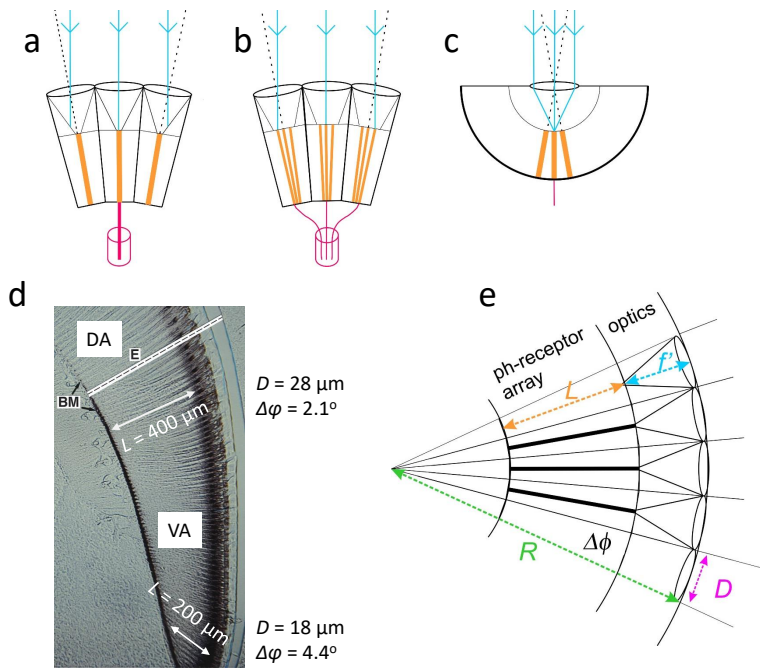

Figure 1: Eye structure and geometry defines resolution and costs. a) Fused rhabdom apposition eye, photoreceptors coding a pixel form fused rhabdom and send axons to a single neural module; b) neural superposition (NS) apposition eye, photoreceptor forms its own rhabdomere, photoreceptors with same optical axes code single pixel and send axons to single neural module; c) simple eye, as in a camera each photoreceptor codes a single pixel. d) Gradient of investment in spatial acuity: apposition eye, honeybee drone, *Apis mellifera*. From ventral to dorsal, lens diameter D increases and interommatidial angle $\Delta\phi$ decreases to increase spatial resolution, and rhabdom length, L, increases to increase SNR_{ph}. 10 µm thick longitudinal section, (DA) dorsal eye area (VA) ventral area. BM - retina's basement membrane; E – equator separating dorsal and ventral regions. From Menzel et al., 1991, original micrograph, courtesy of Doekele Stavenga. e) Schematic section of locally spherical apposition eye region. Volumes of optics and photoreceptor array are determined by dimensions that constrain the quality of the spatial image coded by photoreceptors: lens diameter D, focal distance f', interommatidial angle $\Delta\phi = D/R$ where R is eye radius, and rhabdom(ere) length L.

Because V_o is a specific measure, volume per unit solid angle of visual space, we can compare investments in eye regions that differ in radius and angular extent. Thus V_o handles the regional variations in R observed in many compound eyes.

To simplify our expression for V_o (Equation 1) we fix lens F-number, $F = f/D$ and apply the formula for image formation by a convex cornea, $f' = f.n_i$ where n_i is the refractive index of the internal medium (Nilsson & Land, 2012). This formula describes several apposition eyes, including fly NS eyes (Rossel, 1979; Stavenga, 2003a; Stavenga et al., 1990; Zeil, 1983). Thus

$$V_o = \frac{1}{3}[R^3 - (R - Fn_iD)^3] \ \mu\text{m}^3\,\text{sr}^{-1} \tag{2}$$

We use values measured in blowfly, $F = 2.0$ (Stavenga, 2003a) and $n_i, = 1.34$, (Seitz, 1968).

Fixing F both simplifies our models by reducing the number of free parameters

and accounts for the dependence of the photon flux entering an ommatidium on D by making image brightness (the flux per unit area of rhabdomere entrance aperture) independent of D. We use the specific volume of optics, V_o, as our measure of the cost of optics, C_o $\mu m^3 sr^{-1}$. This usage assumes that the cost of materials, the cost of metabolic energy for maintaining function, and the energy cost of carriage all increase in equal proportion to volume, in all parts of the dioptric apparatus, namely the corneal lens, cone, and surrounding pigment cells. Given the lack of definitive data on composition and costs, this assumption is a reasonable starting point (Discussion).

Calculating the benefits and costs of investing in photoreceptors

Investing in photoreceptors buys photoreceptor signal to noise ratio, SNR_{ph}, by reducing the effects of an optical constraint, the Poisson statistics of photon absorption (Nilsson & Land, 2012), and at higher light levels a physiological constraint, the saturation of a photoreceptor's transduction units - its light sensitive microvilli (Heras & Laughlin, 2017; Howard et al., 1987; Song et al., 2012). A microvillus contains rhodopsin molecules, the intermediate molecules of the phototransduction cascade and the ion channels they activate, and it uses these to generate a brief pulse of depolarising current, a quantum bump, following the activation of a single rhodopsin molecule by an absorbed photon. This all-or-none response takes time to complete, during which the microvillus cannot respond to the absorption of another photon (Hardie & Postma, 2008; Song & Juusola, 2014). Therefore, as light intensity rises to daylight levels, SNR_{ph} falls below the Poisson limit because a photoreceptor's transduction units saturate (Howard et al., 1987). At any given time a significant fraction of microvilli are failing to respond to the absorption of a photon by rhodopsin because they are already engaged in processing a bump. Consequently the transduction rate ψ no longer increases linearly with the absorption rate, and bump statistics change from Poisson to binomial. In daylight, flies activate a photomechanical response, a longitudinal pupil, to prevent excessive saturation and maintain SNR_{ph} close to the maximum permitted by binomial statistics,

$$SNR_{ph} = \frac{1}{2}\sqrt{N_{vil}} \tag{3}$$

where SNR_{ph} is defined with respect to a signal of unit contrast (Howard et al., 1987). Note that by operating at this upper limit the fly obtains maximum benefit from investing in N_{vil}. Thus the benefit of investing in a longer rhabdomere is an increase in SNR_{ph} in bright light, according to

$$SNR_{ph} = \frac{1}{2}\sqrt{\nu L} \tag{4}$$

where L is rhabdomere length and ν is the number of microvilli per unit length. We assume ν is constant along the rhabdomere and from published results we estimate $\nu = 230\,\mu m^{-1}$ (Methods). We acknowledge that diameter, cross section and taper often vary within and among rhabdomeres. We are fixing ν at a plausible value for a generic model.

The cost of increasing SNR_{ph} by increasing L is easily calculated. In fly NS eyes, L is also the depth of the photoreceptor array because the rhabdomeres of

the six largest photoreceptors, R1-6, stretch from the focal plane of the lens to the basement membrane (Hardie, 1985). Thus in a locally spherical eye region (Figure 1) the photoreceptor array's specific volume is

$$V_{ph} = \frac{1}{3}[(R - f')^3 - (R - f' - L)^3] \ \mu\text{m}^3\,\text{sr}^{-1} \tag{5}$$

Substituting $f' = F.n_i.D$

$$V_{ph} = \frac{1}{3}[(R - Fn_iD)^3 - (R - Fn_iD - L)^3] \ \mu\text{m}^3\,\text{sr}^{-1} \tag{6}$$

According to eye geometry (Figure 1), the total specific volume of an eye region is

$$V_{tot} = V_o + V_{ph} \ \mu\text{m}^3\,\text{sr}^{-1} \tag{7}$$

Observe that because both V_o (Equations 1 & 2) and V_{ph} (Equations 5 & 6) depend upon R and $R = D/\Delta\phi$, both V_o and V_{ph} increase with the number of ommatidia per unit solid angle.

For the photoreceptor array we assume that the costs of space, materials and energy for carriage increase in proportion to volume with the same constants of proportionality as optics. Again, in the absence of measurements this assumption is a reasonable starting point (Discussion). However, this assumption breaks down when we consider specific metabolic rates. To enable and power phototransduction, a photoreceptor has an exceptionally high specific metabolic rate (energy consumed per gram, and hence unit volume, per second) (Laughlin et al., 1998; Niven et al., 2007; Pangršič et al., 2005). We account for this extra cost by applying an energy surcharge, S_E. To equate with our other estimates of cost this surcharge has units of $\mu\text{m}^3\,\text{sr}^{-1}$, and we assume that it increases in proportion to N_{vil} because N_{vil} determines the magnitude of the photoreceptor's light-gated conductance (Hardie & Postma, 2008; Heras & Laughlin, 2017). We satisfy these two requirements by defining

$$S_E = K_E N_{vil} \ \mu\text{m}^3\,\text{sr}^{-1} \tag{8}$$

where K_E, the photoreceptor energy tariff, converts the energy consumed by a photoreceptor per microvillus into an equivalent volume.

We estimate K_E (Methods) by adopting the method used to estimate the energy cost of weapons carried by flying beetles (Goyens et al., 2015). We divide the energy consumed per microvillus by the animal's mass specific metabolic rate, SMR, to obtain an equivalent body mass which, assuming a density of 1.0, is our volume equivalent, K_E μm^3 per microvillus. K_E is at present poorly determined: it depends upon several ecological, physiological and behavioural factors, it will vary among species and among individuals of the same species, and there is barely enough data (Methods). Given this uncertainty, we model a range of values from $K_E = 0$ to $K_E = 0.64$ that covers the range we estimate for blowfly, $K_E = 0.13$ to $K_E = 0.52$ (Methods).

To summarise costs, for the photoreceptor array

$$C_{ph} = V_{ph} + S_E \ \mu\text{m}^3\,\text{sr}^{-1} \tag{9}$$

and for the optics

$$C_o = V_o \ \mu\text{m}^3\,\text{sr}^{-1} \tag{10}$$

Because C_o and C_{ph} have the same units and are specific (per unit solid angle), we can transfer resources between optics and photoreceptors within the constraint of total specific cost

$$C_{tot} = C_o + C_{ph} \ \ \mu\text{m}^3\,\text{sr}^{-1} \tag{11}$$

Modelling the effects of resource allocation on NS eye performance

When C_{tot} is fixed, allocating a smaller proportion to optics and a larger proportion to photoreceptors trades the benefits of investing in optics for the benefits of investing in photoreceptors (Figure 2).

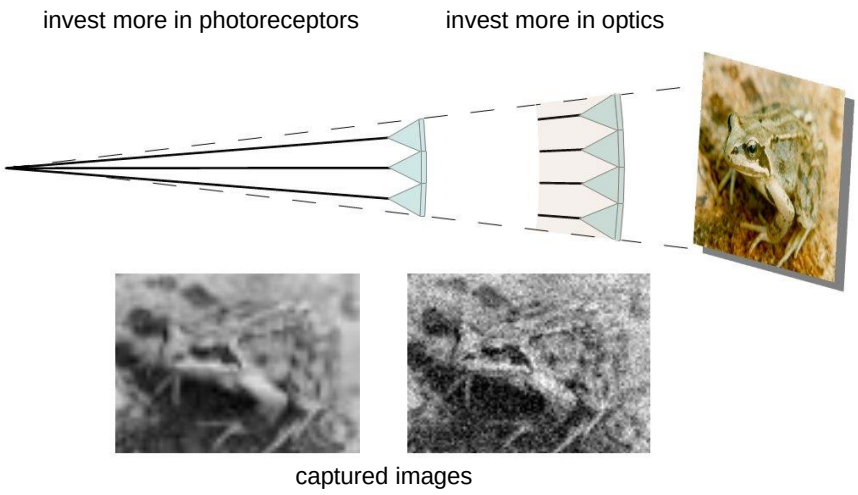

Figure 2: The effect of trading investment in photoreceptor array for investment in dioptric apparatus. Schematic shows two eye regions of equal specific volume, the left investing more heavily in photoreceptors, the right more heavily on optics. The images they capture show that transferring resources from photoreceptor array to optics increases image sharpness and contrast at the expense of increasing noise.

Having used constraints to link investments in dioptrics and photoreceptor array to three major determinants of the quality of the achromatic images captured by fly photoreceptors R1-6, namely $\Delta\rho$, $\Delta\phi$ and SNR_{ph}, we can now model how trade-offs between optics and photoreceptors change an eye's ability to support vision. Several measures of visual performance depend on $\Delta\rho$, $\Delta\phi$ and SNR_{ph}. To establish proof of principle we use a general measure that embraces a wide variety of resolvable achromatic image details - spatio-temporal information capacity in bits sr^{-1} s^{-1}. Information capacity has proved useful for measuring the performance of compound eyes (de Ruyter van Steveninck & Laughlin, 1996), discovering design principles (Howard & Snyder, 1983; Snyder et al., 1977; van Hateren, 1992), and illuminating the evolution of simple eyes (Nilsson & Pelger, 1994). The measure is particularly

relevant for a fly NS eye because coding by second order neurons is adapted to maximise information capacity (Laughlin, 1981; van Hateren, 1992).

To model the effects of resource allocation on information capacity, we fix C_{tot} and generate pairs of D and L that cover the range of values permitted by eye geometry. Each D, L pair specifies an investment in optics, $C_o(D, L)$, an investment in photoreceptors $C_{ph}(D, L)$ and hence the three determinants of image quality, $\Delta\rho(D, L)$, $\Delta\phi(D, L)$, and $SNR_{ph}(D, L)$, that specify spatio-temporal information capacity $H(D, L)$ bits sr^{-1} s^{-1}.

We calculate $H(D, L)$ (Methods) in the frequency domain (Howard & Snyder, 1983; van Hateren, 1992). In brief, a 2-D power spectrum typical of natural scenes is low-pass filtered by the photoreceptor angular sensitivity function, $\Delta\rho(D, L)$, and sampled by an hexagonal lattice of photoreceptors specified by $\Delta\phi(D, L)$. Movement of the retinal image modulates the flux of photons entering a photoreceptor by converting spatial frequencies into temporal frequencies, according to the distribution of angular velocities generated during behaviour. Then during transduction, the photoreceptors low-pass filter these temporal frequencies and add the noise generated by sampling the photon flux stochastically with transduction units (microvilli). We use van Hateren's (1992) formulae for the $1/f^2$ power spectrum of natural scenes and the distribution of image velocities appropriate for blowfly, and we temporally low pass filter according to the measured properties of a fully light-adapted blowfly photoreceptor R1-6 (Methods). We also modify van Hateren's method to take account of the spatial aliasing that occurs when an array of ommatidia undersamples an image (Methods).

By calculating information capacities for each D, L pair we define the performance surface $\boldsymbol{H(D, L)}$ that covers the morphospace of model eyes of given F-number, F, and specific cost, C_{tot}. The performance surface is a flat-topped ridge with steep flanks (Figure 3). Atop the ridge, a single point of maximum capacity, $H(D_{opt}, L_{opt})$, sits in an extensive zone within which capacity, and hence efficiency, is $> 95\%$ maximum (red zone in Figure 3). With efficiency dropping steeply away from the ridge, approximately two thirds of D, L combinations have efficiencies $< 70\%$. The shape of the performance surface depends upon photoreceptor energy cost (Figure 3). Increasing the energy tariff K_E reduces L_{opt} from the maximum permitted by eye geometry to one quarter of maximum. However, because the ridge is flat-topped, L_{opt} still lies in an extensive high-efficiency zone, within which L can be changed three-fold and D by 40%, while maintaining $> 95\%$ efficiency (Figure 3). This broad high-efficiency zone is bad news for investigators who set out to establish that eyes are optimised, but good news for insects. An eye region can be adapted for a specific purpose, e.g. by increasing L to increase SNR, without sacrificing more than 5% of a measure of general-purpose vision, information capacity. Thus this robust region of design space can facilitate evolution by reducing loss of function.

Patterns of investment in optimised NS eye models

We next establish how, in theory, eye structure and investments in optics and photoreceptor array vary with total investment when efficiency is optimised by maximising information capacity. We run our fly NS eye model with different combinations of C_{tot} and K_E and for each combination find the values of L_{opt}, D_{opt} and $\Delta\phi_{opt}$ that maximise information capacity and the corresponding investments in optics

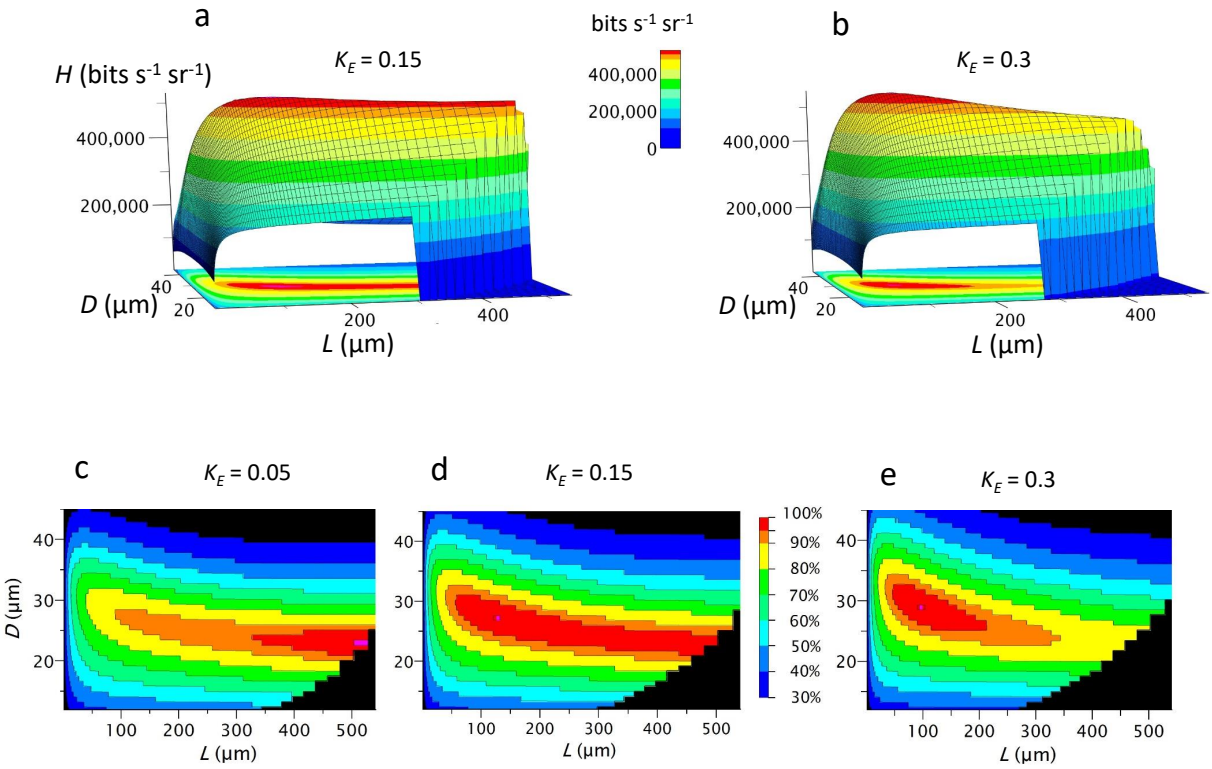

Figure 3: The performance surface $\boldsymbol{H(D,L)}$ describes how information capacity changes across all geometrically permissible configurations of an eye of fixed cost - the eye's morphospace. Red area: high-performance zone in which capacity is > 95% maximum. Surfaces plotted for model fly neural superposition (NS) eyes, with F-number, $F = 2$ and total cost, $C_{tot} = 4 \times 10^9\,\mu\text{m}^3\,\text{sr}^{-1}$ at 3 values of photoreceptor energy tariff K_E. Acceptance angle $\Delta\rho$ calculated using Snyder's (1979) CoG approximation.

and photoreceptor array, C_o and C_{ph}. For each combination of C_{tot} and K_E we run two versions of our NS model, one calculates $\Delta\rho$ using CoG (Snyder, 1979) and the other WOM, which produces a narrower $\Delta\rho$ that comes closer to the lens diffraction limit (Stavenga, 2004a). The two versions give similar patterns of investment (Figure 4).

Rhabdomere length is matched to acuity and rhabdomeres are long

As C_{tot} increases, D_{opt} widens to increase lens contrast transfer and resolving power by reducing $\Delta\rho$, $\Delta\phi_{opt}$ narrows to increase spatial resolution, and L_{opt} lengthens to improve SNR_{ph}, reaching several hundred microns in larger eyes (Figure 4a,b,c) Thus efficient resource allocation can, in theory, explain why NS eye rhabdomeres are long and rhabdomere length increases with spatial acuity. Note that improving the performance of the optical system by approaching the lens diffraction limit to resolving power improves an eye's performance in full daylight. With the WOM approximation for $\Delta\rho$ the lens diameter D required to achieve a given $\Delta\rho$ is decreased,

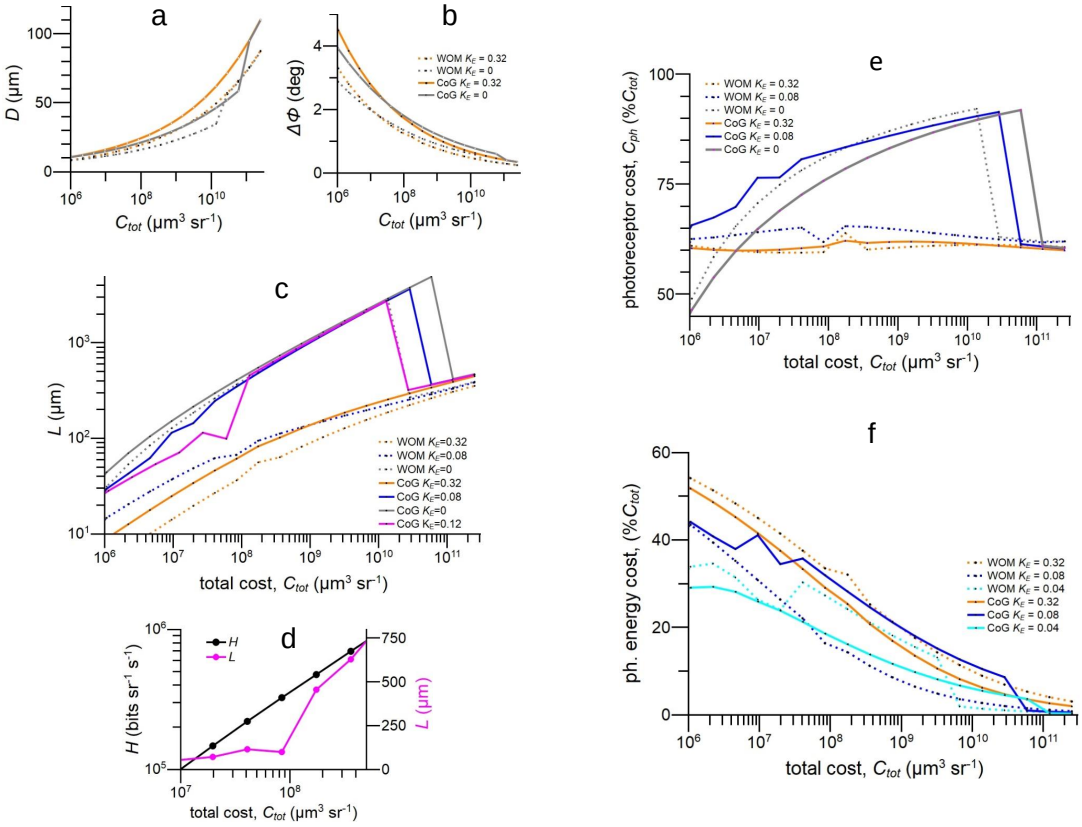

Figure 4: When model fly NS eyes are optimised for information capacity, eye structure, eye performance and the division of resources between optics and photoreceptor array depend on total investment, C_{tot} and photoreceptor energy tariff, K_E. a) lens diameter D; b) interommatidial angle, $\Delta\phi$; c) rhabdomere length, L. Note that sudden jump in the curve for CoG $K_E = 0.12$. d) optimum information capacity H and rhabdomere length L at CoG $K_E = 0.12$ plotted over the range of C_{tot} within which L jumps upward. The eight-fold increase in L has very little effect on the rate of increase of H. e)%C_{tot} allocated to photoreceptor array; f) photoreceptor energy cost as %C_{tot}. CoG, acceptance angle approximated by convolving Gaussians (Snyder, 1979); WOM, acceptance angle approximated according to wave optics model (Stavenga, 2004a). Key in b) also applies to a).

and this allows $\Delta\phi$ to decrease (Figure 4b), thereby increasing the spatial resolution achieved by an efficient eye of given total cost.

Photoreceptor energy cost changes the structure of an efficient eye

Increasing the photoreceptor energy tariff K_E has little effect on the optimum values of D and $\Delta\phi$, but it reduces the optimum value of L, and hence the depth of the photoreceptor array, by as much as 90% (Figure 4c). The optimum value of L is most sensitive to K_E in the range 0.04 to 0.16. and tends jump up and down as C_{tot} increases. Careful interrogation of our MATLAB code suggests that coding and rounding errors are not responsible for these jumps. We attribute the jumps to interactions between competing non-linear terms (e.g. the dependence on contrast signal on D, noise on $L^{0.5}$, information on $\log(SNR)$, effective spatial bandwidth on $R^{0.5}$, volume on R^3) that shift the optimum across a flat-topped performance

surface. This explanation is supported by the observation that these large jumps in optimum L have very little effect on the optimum information rate (Figure 4d). The effects of K_E on eye structure are also sensitive to optical performance: increasing K_E has a greater effect on L_{opt} in the more sharply focussed WOM model at all but the highest values of C_{tot} (Figure 4c). As expected, increasing K_E reduces the spatial resolution achieved at a given C_{tot} by reducing the resources available for investment in the volume costs V_o and V_{ph}.

Photoreceptor arrays are allocated more resources than optics

When our NS eye models are optimised for information capacity, more than 50% of C_{tot} is allocated to photoreceptor arrays over the range $C_{tot} = 2 \times 10^6$ to $3 \times 10^{11}\,\mu m^3\,sr^{-1}$, irrespective of optical effectiveness (CoG c.f. WOM) and photoreceptor energy tariff, K_E (Figure 4e). At lower values of K_E, the optimum allocation to photoreceptor arrays is strongly dependent on C_{tot}, increasing from 45% to 90% C_{tot} over the range $C_{tot} = 1 \times 10^6\,\mu m^3\,sr^{-1}$ to $1 \times 10^{10}\,\mu m^3\,sr^{-1}$, and then jumping down to approximately 60% between $C_{tot} = 1 \times 10^{10}\,\mu m^3\,sr^{-1}$ and $C_{tot} = 1 \times 10^{11}\,\mu m^3\,sr^{-1}$ (Figure 4e). At higher values of K_E, the optimum photoreceptor allocation is relatively insensitive to C_{tot} and lies between 60% C_{tot} and 65% C_{tot}. We conclude that, in theory, the cost of the photoreceptor array is as significant as the cost of optics. Therefore to fully understand eye design both costs must be taken into account.

The relative contributions of photoreceptor array volume, V_{ph}, and photoreceptor energy cost, S_E, to total array cost, C_{ph}, depends on total investment, C_{tot} (Figure 4f). At our lowest C_{tot}, i.e. in the lowest acuity eyes regions, the energy cost is 25% to 50% of C_{tot}, depending on K_E, but as eye size increases the costs associated with array volume come to dominate and photoreceptor energy cost drops to 5% of C_{tot}.

Flies invest efficiently in costly photoreceptor arrays

Our new method for calculating costs enables us to estimate, for the first time, the total investment an animal makes in an eye or eye region, and break this down into its two major components, optics and photoreceptor array. Using published measurements of D, $\Delta\phi$ and L we determine the specific volumes of dioptric apparatus, V_o, and photoreceptor array, V_{ph} in fly neural superposition (NS) eyes. Although numerous publications give values of D and $\Delta\phi$ (Feller et al., 2021; Land, 1997), very few include L. We have values for just 12 eye regions, taken from 7 species of flies (Table 2). For each region we insert the values, L, D, $\Delta\phi$ and f', into Equations 1 and 5 to calculate V_o, V_{ph}, and V_{tot}. Where focal distance f' is not reported (Table 2), we follow our models (Equation 2) and calculate $f' = FDn_i$ with $F = 2$ and $n_i = 1.34$.

The 12 eye regions provide a well-distributed set of empirical values of L, D, $\Delta\phi$, V_o, V_{ph} and V_{tot} that spans almost five orders of magnitude of V_{tot}, from $1.4 \times 10^6\,\mu m^3\,sr^{-1}$ and $2.1 \times 10^6\,\mu m^3\,sr^{-1}$ for the low acuity eye region of the March fly *Dilophus febrilis* and the eye of *Drosophila melanogaster* respectively, to $9 \times 10^{10}\,\mu m^3\,sr^{-1}$ for the remarkable fovea of the small robber fly *Holcocephala fusca* (Wardill et al., 2017).

We compare the empirical values obtained from flies with theoretical curves, obtained from model NS eyes that are optimised for information capacity (Figure 5). Note that for our theoretical curves we plot D, $\Delta\phi$, L and V_{ph} against total specific

species	eye region	D µm	$\Delta\phi$ deg	L µm	f µm	f' µm	F	source
Calliphora vicina	male acute zone	37	1.07	340	74	99	2	1,2,3,4
Calliphora vicina	female acute zone	29	1.28	280	58	78	2	2
Musca domestica	male love spot	36	1.75	250	72	96	2	2,5
Musca domestica	male peripheral	20	3.5	140	40	54	2	2
Drosophila melanogaster	average	16.5	5	83	20	27	1.25	1,2,6
Coenesia attenuata	female frontal	20	2.3	140	25	28	1.25	7
Bibio marci	male dorsal	33	1.6	230	70	94	2.1	8
Bibio marci	male ventral and female	21	3.7	110	36	48	1.7	8
Dilophus febrilis	male dorsal	24	2.2	180	40	54	1.7	8
Dilophus febrilis	male ventral and female	15	5.1	60	16	21	1.1	8
Holcocephela fusca	acute zone, max. acuity	75	0.28	230	160	176	2.53	9
Holcocephela fusca	peripheral	21	3.5	123	33	45	1.6	9

Table 1: Measurements of Dipteran neural superposition (NS) eyes, extracted from published sources, 1. Land 1997; 2. Hardie 1985; 3. Stavenga et al. 1990; 4. Stavenga 2003a; 5. Land and Eckert 1985 ; 6. Stavenga 2003b; 7. Gonzalez Bellido et al. 2011; 8. Zeil 1983; 9. Wardill et al. 2017. Further details of the measurements used and results obtained are given in supplementary table S1.

cost, C_{tot} µm^3 sr^{-1} (Figure 4). This total includes the surcharge for photoreceptor energy consumption S_E µm^3 sr^{-1}, which increases in proportion to the number of microvilli and the photoreceptor energy tariff, K_E (Equation 8). However, we cannot estimate C_{tot} in flies because their values of K_E are not well-determined (Methods). Although K_E will vary considerably between species, we only have enough published data to calculate its order of magnitude and likely range (Methods). Furthermore, K_E is species-specific and, because we have no more than two data points per species and we are using a generic model that does not account for differences in d_{rh} and F among species (Table 2), we cannot estimate K_E by fitting our model to the empirical data. For these reasons we compare theoretical findings to empirical data by plotting them against a measure of eye size that is both calculated by our models and estimated from data, total specific volume, V_{tot}. Because K_E is uncertain, we plot theoretical curves calculated with values of K_E from within our likely range.

Looking across 12 fly eye regions, D increases and $\Delta\phi$ decreases as V_{tot} increases. D lies within, or close to, the theoretical envelope defined by CoG models optimised with $K_E = 0$ and $K_E = 0.32$ (Figure 5a), and tends to slightly exceed optimum

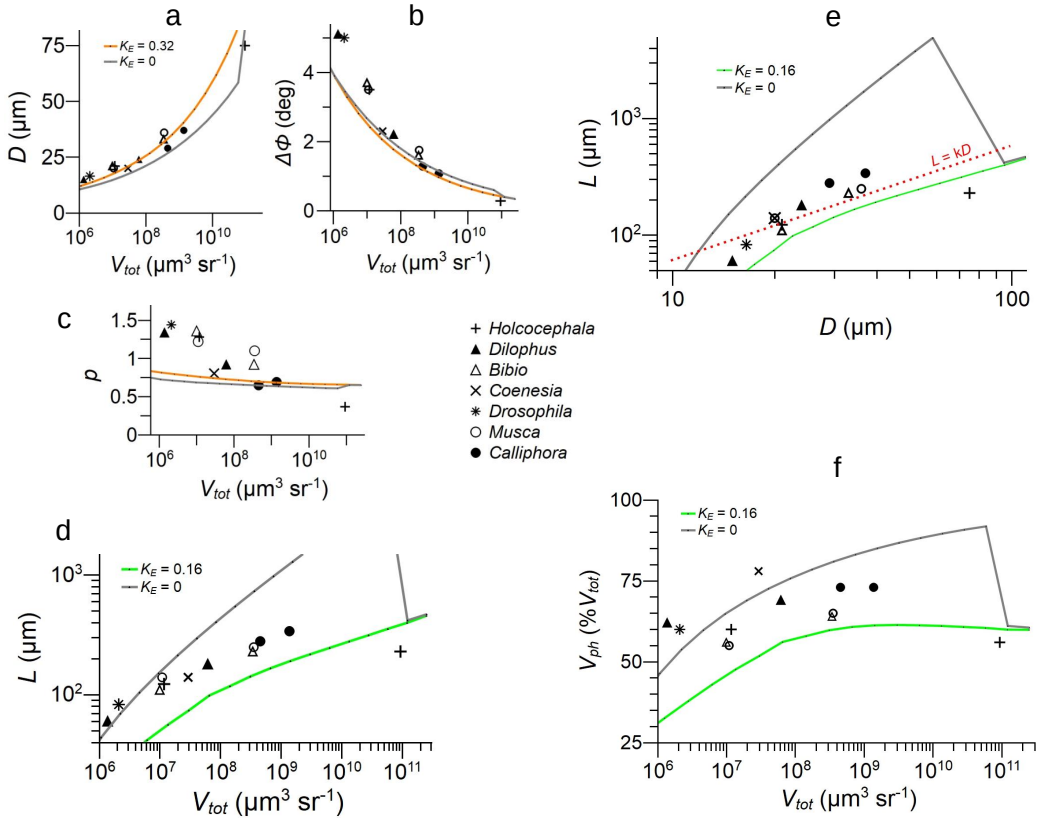

Figure 5: Parameters defining the configurations of 12 fly NS eye regions, taken from 7 species (Table 2), compared to model NS eyes optimised for information capacity at given values of photoreceptor energy tariff K_E, and total specific volume V_{tot}. a) lens diameter D, b) interommatidial angle $\Delta\phi$ and c) eye parameter $p = D\Delta\phi$ (keys as in a), d) rhabdomere length L. e) Log-log plot of L vs D, dashed line shows slope for isomorphic scaling, $L \propto D$;. f) Specific volume of photoreceptor array, V_{ph} expressed as % total specific volume of eye, $\%V_{tot}$. Models use Snyder's CoG approximation for photoreceptor acceptance angle (Snyder, 1979).

values at lower specific volumes. $\Delta\phi$ is approximately 25% wider than optimum (Figure 5b) in the four eye regions with lowest specific volume and close to optimum elsewhere. The eye parameter, $p = D\Delta\phi$, (Figure 5c) indicates the degree to which an apposition compound eye sacrifices spatial resolution by sampling below the lens diffraction limit. Only *Holcocephala* fovea, $p = 0.37$, comes close to the diffraction limit $p = 0.29$ (Snyder, 1979). As observed in a number of diurnal apposition eyes (Wehner, 1981), the remaining 11 fly eye regions in our data set undersample by a factor of 2 or more, with p decreasing with increasing V_{tot} from 1.4 to 0.65 (Figure 5c). Our optimised models also undersample, with p decreasing with increasing V_{tot} from 0.89 to 0.65 (Figure 5c). Note that like D and $\Delta\phi$, p is relatively insensitive to K_E. We conclude that in most eye regions p is not optimised for spatio-temporal information capacity, at least according to our model, because it is higher than predicted at all but the highest values of V_{tot}.

Rhabdomere length, L, increases with V_{tot} from 60 µm to 340 µm (Figure 5d; Table 2), within or close to the theoretical envelope defined by $K_E = 0$ and $K_E = 0.16$. There is a robust trend: the empirical values of log L increase with log V_{tot},

and hence with increasing D and decreasing $\Delta\phi$ (Figure 5a,b), along a trajectory that resembles theoretical curves for optimum log L. However, the data do not follow the theoretical curve for any particular value of K_E, and there is some scatter among the data points (Figure 5d). We have three reasons to attribute most of this scatter to unknown differences in K_E. First, the optimum value of L is sensitive to K_E (Figure 4c); second, K_E will vary between species (Methods); and third, the empirical values of D and $\Delta\phi$, which are in theory relatively insensitive to K_E, are less scattered and lie closer to our theoretical predictions (Figure 5a,b). The one obvious outlier, the shorter than predicted rhabdomeres in *Holcocephala* fovea (Figure 5d), is easily explained: the optics and photoreceptor array of this forward pointing fovea, together with underlying optic lobe, are tightly packed into a head that is less than 600 µm from front to back (Wardill et al., 2017), and this lack of headroom limits the depth of the eye, $(L + f')$.

The log-log plot of L versus D (Figure 5e) shows that the increase in L with V_{tot} is not explained by proportional scaling because the empirical values do not lie on a straight line of slope 1, $L = \mathrm{k}D$. As expected of a physiological system subject to several competing constraints (G. K. Taylor & Thomas, 2014), the theoretical curve continuously changes slope, and this is reflected in the data. Thus the matching of L to D and $\Delta\phi$ observed in the data is not the consequence of a simple developmental constraint, it is the product of developmental mechanisms that allocate resources efficiently to optics and photoreceptor array.

We conclude that the eye regions we analyse are, according to our generic model, not optimised for spatio-temporal information capacity because the data points that are least sensitive to the photoreceptor energy tariff K_E, namely D, $\Delta\phi$ and p, are generally larger than predicted. Nonetheless, we argue on two grounds that the matching of rhabdomere length to spatial resolution seen in flies promotes the efficiency of their total investments in eye. L lies within, or close to, the theoretical envelope predicted by models optimised for efficiency, and because the theoretical performance surface has a wide flat high-efficiency zone (Figure 3), large deviations from optimum have relatively little impact on efficiency.

To accommodate photoreceptors' lengthy rhabdomeres, flies allocate between 56% and 78% of eye volume, V_{tot}, to photoreceptor arrays (Figure 5f). The smaller remainder, between 44% and 22%, is allocated to optics. There is a slight trend for the percentage allocated to photoreceptors to increase with V_{tot}. With the exception of *Holcocephala*'s fovea, where the depth of the photoreceptor array is much less than predicted for optimum allocation, the volumes allocated to photoreceptor arrays lie within or close to the theoretical envelope defined by $K_E = 0$ and $K_E = 0.16$. On this basis we conclude that our diurnal flies allocate a larger fraction of eye volume to photoreceptors than to optics, and this allocation promotes the efficient use of resources. Thus photoreceptor costs are playing a major role in determining the design and efficiency of flies' NS eyes.

Fused rhabdom apposition eyes show similar patterns of investment

We investigate diurnal apposition eyes with fused rhabdoms by modifying our NS eye model and comparing theoretical results with empirical data using the procedures developed for NS eyes. The modifications are straightforward. We increase lens

F-number to 5.5 and reduce d_{rh} to 1.8 µm. These values are in the middle of the wide range found in our sample of apposition eye regions (Table 3). We also adjust the relationship between L and the number of microvilli N_{vil} to account for a fused rhabdom (Methods). For simplicity we assume that all photoreceptors contribute equal numbers of microvilli along the full length of the rhabdom so that N_{vil} increases in proportion to the depth of the photoreceptor array.

species	**eye region**	***D*** µm	$\Delta\phi$ deg	***L*** µm	***f*** µm	***f'*** µm	***F***	**source**
Tenodora australasiae	eye coordinates z=15;x=20 (fovea)	47.5	0.64	500	205	445	8	1
	z=15;x=30	51.5	0.8	535	335	405	6.5	1
	z=15;x=10	41	1	415	305	375	7.4	1
	z=15;x=0	35	1.1	285	205	275	5.9	1
	z=15;x=60	42	1.6	390	150	212	3.6	1
	z=15;x=100	33	2.5	330	110	153	3.3	1
Sympetrum spp.	ventral -60 deg	31	1.85	461	124	166	4	2
	ventral -5 deg	27	1.75	461	108	148		2
	dorso-ventral border	31	1.69	516	124	167		2
	dorsal +50	53	1.82	627	92	123		2
	dorsal +70	61.5	1.78	886	246	330	4	2
	dorsal fovea	71	0.35	1107	305	410	4.4	2
Apis mellifera drone	dorsal eye	40	1	500	205	275	5.1	3
	top ventral	28	2.1	400	145	194	5.1	3
	mid ventral	25	2.8	280	82	110	3.3	3
	basal ventral	18	4.4	150	54	72	3	3
Apis mellifera worker	max. acuity	25	1.6	350	100	134	5.6	4,5

Table 2: Measurements of fused-rhabdom apposition eyes, extracted from published sources, 1. Rossel 1979; 2. Labhart and Nilsson, 1995; 3. Menzel et al 1991; 4. Varela and Wiitanen, 1970; 5. Kelber and Somanathan, 2019. Details of measurements are given in supplementary table S1.

We then compare the models' predictions of the optimum values of $L, D, \Delta\phi, V_o, V_{ph}$ and V_{tot} with empirical values extracted from published measurements of $D, \Delta\phi, L$ and f', (Table 3). The necessary data is only available from studies of four species: the mantid *Tenodera australis* (Rossel, 1979), the honeybee *Apis mellifera* (Kelber & Somanathan, 2019; Menzel et al., 1991; Varela & Wiitanen, 1970), and two species of the Libellulid dragonfly *Sympetrum* that are so similar that their data are lumped together (Labhart & Nilsson, 1995). The studies provide empirical values for 16 eye regions, which span a range of V_{tot}, from $4.4 \times 10^7\,\mu m^3\,sr^{-1}$ for *Apis* worker ventral eye to $1.8 \times 10^{11}\,\mu m^3\,sr^{-1}$ for *Sympetrum* dorsal fovea (Figure 6).

Looking across our limited sample of fused rhabdom apposition eyes, D increases with V_{tot}, $\Delta\phi$ decreases, and L increases from 280 µm to 1100 µm (Figure 6a,b,c). These empirical values are more widely scattered than those for NS eyes (Figure 5a,b,d), and the discrepancies between empirical and predicted values are larger. We expect a wider scatter because our sample of fused rhabdom eyes is more diverse than our sample of NS eyes, both structurally and phylogenetically. In addition,

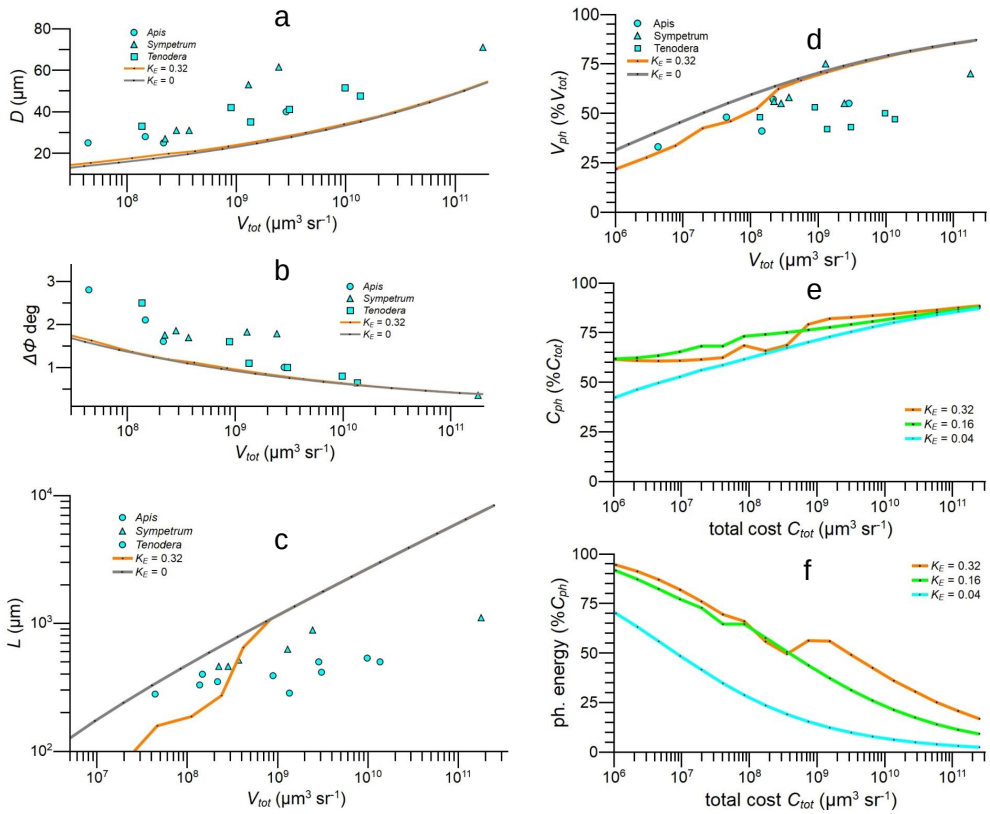

Figure 6: Theoretical results from apposition eye models optimised for information capacity compared to empirical data from 16 apposition eye regions taken from 3 species (Table 3). a) D vs specific volume V_{tot}; b) $\Delta\phi$ vs V_{tot} c) L vs V_{tot}; d) photoreceptor array specific volume V_{ph} as $\%V_{tot}$ vs V_{tot}. (e & f) Models demonstrate impact of photoreceptor costs and its dependence on total cost, C_{tot}. e) Photoreceptor cost, C_{ph}, as $\%C_{tot}$; f) Photoreceptor energy cost as $\%C_{ph}$. Models run with F-number $F = 5.5$, using COG approximation for acceptance angle (Snyder, 1979) and values of energy tariff K_E given in keys.

the scatter is dominated by regional differences within eyes (Figure 6), several of which adapt a region for a specific task. For example, the 1100 µm rhabdomeres of the dragonfly *Sympetrum*, which are the longest photoreceptive waveguides found in any eye, adapt the fovea for detecting small prey against a bright blue sky by enhancing SNR_{ph} (Labhart & Nilsson, 1995). Despite the scatter in data points, fused rhabdom eyes follow the trends seen in NS eyes (Figure 6 c.f. Figure 5). In most eye regions, D and $\Delta\phi$ are larger than predicted by models optimised for efficiency (Figure 6a,b), so therefore is the eye parameter p (values not plotted). At low V_{tot}, L lies within the theoretical envelope defined by models run with plausible values of photoreceptor energy tariff, K_E. However, at higher specific volumes L falls increasingly short (Figure 6c). As with flies' NS eyes, large investments are made in photoreceptor arrays. The volume fractions of photoreceptor arrays increase from 33% V_{tot} to 75% V_{tot} as V_{tot} increases, and the majority of values lie between 40% V_{tot} and 60% V_{tot} (Figure 6d). Our information maximisation models predict an increase from 33% V_{tot} to 85% V_{tot}.

Our models also give the relative contribution of photoreceptor cost to total cost when fused rhabdom apposition eyes are optimised for spatial information capacity.

The percentage of total investment devoted to the photoreceptor array increases with the energy tariff K_E and climbs steadily with increasing C_{tot}, from 43% to more than 80% (Figure 6e). As in NS eyes, the contribution of photoreceptor energy consumption to array cost is progressively marginalised by array volume cost as C_{tot} increases, falling to less than 20% in the largest eyes (Figure 6f).

We conclude that the 16 eye regions in our sample of fused rhabdom apposition eyes are not optimised for spatio-temporal information capacity, at least according to our models. However, the regions exhibit three trends that are associated with efficient resource allocation - rhabdomeres are relatively long, length increases with acuity, and the photoreceptor array occupies a large fraction of eye volume. These trends suggest that, as in NS eyes, resources are being divided between optics and photoreceptor array to promote efficiency, consequently photoreceptor costs play a major role in the design of fused-rhabdom apposition eyes.

Patterns of efficient investment are different in simple eyes

To further investigate how investment patterns differ according to eye type, we construct a basic hemispherical model of a simple eye with rhabdomeric photoreceptors (Methods; Figure 7a) that captures the equivalence of D, f' and $\Delta\phi$ in apposition and simple eyes (Kirschfeld, 1976). We then follow the procedures described above to see how optimum patterns of investment depend on total investment, C_{tot}, and photoreceptor energy tariff, K_E. We consider the same 5 orders of magnitude of total investment, $C_{tot} = 1 \times 10^6$ to $2.5 \times 10^{11}\,\mu\text{m}\,\text{sr}^{-1}$, and for simple eye models this encompasses a 100 fold range of lens diameters, $D = 29\,\mu\text{m}$ to $2.9\,\text{mm}$, and focal distances, $f' = 79\,\mu\text{m}$ to $7.9\,\text{mm}$.

For each C_{tot} there is an optimum division of resources between optics and photoreceptors that maximises information capacity. L_{opt} increases with V_{tot}, scaling close to $(C_{tot})^{1/3}$ (Figure 7b). Increasing the energy tariff, K_E, greatly reduces L_{opt} without changing this scaling exponent. At any given C_{tot} and K_E, L_{opt} is much shorter in simple eyes and the difference increases with C_{tot} from at least 50% shorter at $C_{tot} = 1\times10^6\,\mu\text{m}^3\,\text{sr}^{-1}$ to over 90% shorter at $C_{tot} = 1\times10^9\,\mu\text{m}^3\,\text{sr}^{-1}$. We conclude that, in theory, efficient resource allocation explains why photoreceptors in diurnal simple eyes have much shorter light-sensitive waveguides than photoreceptors in diurnal apposition eyes.

Patterns of investment differ from apposition eyes in other respects (Figure 7). In simple models the optimum volume fraction of the photoreceptor array is insensitive to C_{tot} whereas in apposition models it increases with C_{tot}. In addition, a simple eye is much more sensitive to photoreceptor energy consumption. The small energy tariff, $K_E = 0.04$, reduces simple eye array volume from 35% V_{tot} to 12% V_{tot}, but has a negligible effect on an NS eye. Raising the tariff to $K_E = 0.32$, reduces the simple eye's array volume to just 3% V_{tot} but in apposition models it is always >30% V_{tot}. Despite this ten-fold reduction in $\%V_{tot}$ the total resources allocated to photoreceptor array increases from 35% to 57% (Figure 7d) because the relative contribution of photoreceptor energy consumption increases from 40% C_{tot} to 55% C_{tot}. Finally, in simple eyes the relative contribution of photoreceptor energy consumption is insensitive to C_{tot}, but in apposition models it falls steadily with increasing C_{tot}, to around 5% C_{tot} (Figure 7d). This difference between eye types can be attributed to differences in eye geometry (Figure 7a). As C_{tot} increases, the simple eye maintains

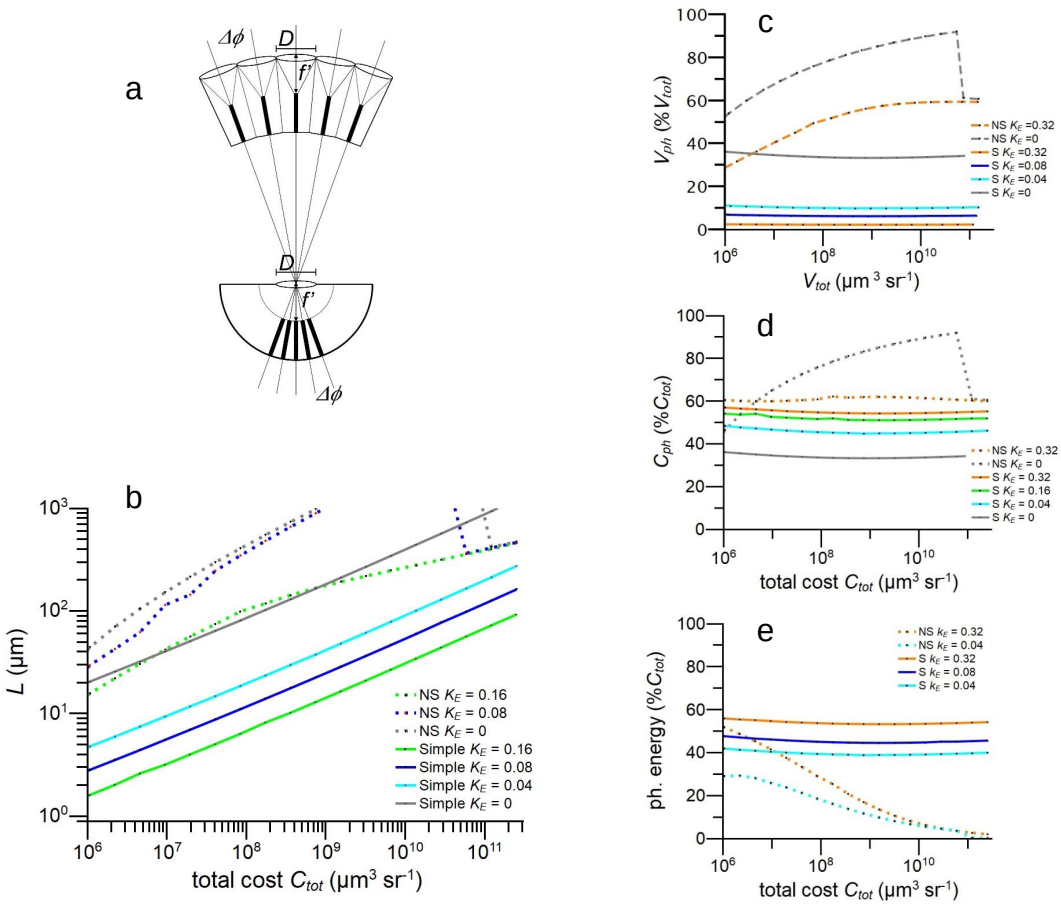

Figure 7: Resource allocation in model simple eyes optimised for information capacity compared to optimised model neural superposition apposition eyes (NS). a) Schematic showing apposition eye and simple eye with identical spatial resolution, as defined by lens diameter D, focal distance f', rhabdom(ere) diameter d_{rh}, and rhabdom(ere) length, L (after Kirschfeld, 1976). Note the denser packing of photoreceptors inside the simple eye. (b - e) Properties of simple and NS eye models optimised for information capacity in full daylight. b) Photoreceptor length, L vs specific volume V_{tot}; c) photoreceptor specific volume V_{ph} expressed as $\%V_{tot}$ vs V_{tot}. d) Photoreceptor investment C_{ph} as $\%C_{tot}$ vs C_{tot}. e) photoreceptor energy cost as $\%C_{tot}$ vs C_{tot}. Models use Snyder's (1979) CoG approximation for acceptance angle.

its dense packing of photoreceptors but an apposition eye's photoreceptors become increasingly widely spaced as larger lenses force the boundaries between ommatidia further apart. We conclude that when resources are efficiently allocated, the differences in geometry that define eye type can profoundly influence both the impact of photoreceptor energy consumption on eye morphology and the distribution of costs within an eye.

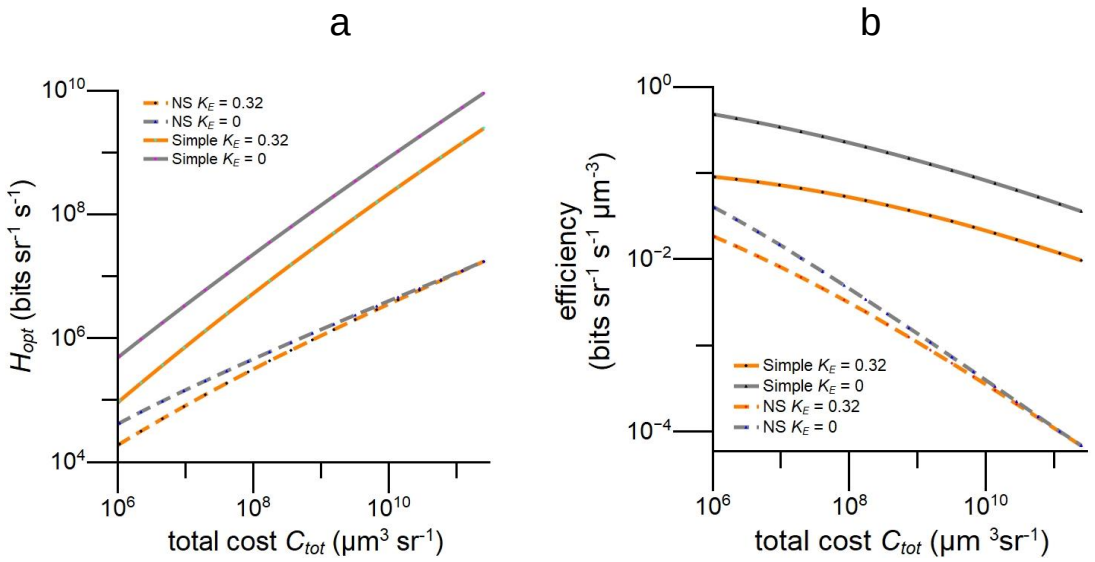

Figure 8: Information rate, H v.s. total cost C_{tot} for simple and apposition model eyes optimised to maximise information capacity in full daylight. a) Rates are higher in simple eyes and more sensitive to photoreceptor energy tariff, K_E b) Efficiency, bits per unit specific volume per second, falls less steeply with increasing C_{tot} in simple eyes. Models use Snyder's CoG approximation (1979) for acceptance angle.

Information capacity and investment

In all optimised eye models, apposition and simple, the spatio-temporal information capacity, H_{opt}, increases sub-linearly with total investment, C_{tot}, (Figure 8a), making a bit of information more expensive in a larger eye. In simple eyes, H_{opt} increases as $(C_{tot})^{0.8}$ across the full range of C_{tot} while in apposition models the exponent is lower, decreasing from 0.6 to 0.5 as C_{tot} increases. Thus the simple eye model is 10 times more efficient when $C_{tot} = 1 \times 10^6\,\mu\text{m}^3\,\text{sr}^{-1}$ and approximately 100 times more efficient when $C_{tot} = 1 \times 10^{11}\,\mu\text{m}^3\,\text{sr}^{-1}$ (Figure 8b). Increasing the photoreceptor energy tariff reduces the efficiency of all eye types, but this effect declines as apposition eye models increase in size (Figure 8b) because, for reasons of geometry, volume costs marginalise photoreceptor energy cost.

Discussion

We initiate a new approach to understanding eye design by investigating how the division of resources between an eye's dioptric apparatus and photoreceptor array influences an eye's performance and efficiency. To achieve this we formulate a new measure of cost, specific volume, that is defined by an eye's shape and the dimensions of its components, can be adjusted to account for the high energy cost of photoreceptors, and relates investments in optics and investments in photoreceptors to three basic determinants of image quality, interreceptor angle $\Delta\phi$, photoreceptor acceptance angle $\Delta\rho$, and photoreceptor signal to noise ratio SNR_{ph}, via optical, geometrical and physiological constraints. These advantages allow us to model how an eye's performance changes when resources are transferred between optics and photoreceptors. Thus we can, for the first time, model performance across the morphospace of an eye of given type and total cost. Using a general-purpose measure of performance, spatio-temporal information capacity (Howard & Snyder, 1983; van Hateren, 1992), we find that the surface for an apposition compound eye (Figure 3) is flat topped - the optimum configuration that maximises performance sits in a broad high efficiency zone in which performance over 95% of maximum. Within this robust region of morphospace an eye, or eye region, can be specialised for a specific task with little loss of information, and this can facilitate evolution by reducing loss of function. Our models predict that efficiently configured diurnal apposition eyes invest heavily in deep photoreceptor arrays with long rhabdomeres and rhabdoms, and match investments in optics and photoreceptor arrays so that rhabdom(ere) length increases with spatial resolution (Figure 4). By applying our new method of costing investments to published data, we show that fast-flying diurnal insects conform to these trends and are, therefore, configured to be efficient (Figures 5, 6). Our models also demonstrate that photoreceptor energy consumption is an important factor in an apposition eye's design and performance: it reduces photoreceptor length by as much as 90% and information capacity by as much as 60%. To see how resource allocation and performance depend on eye type we model a simple (camera type) eye (Figure 7). When optimised for efficiency, a simple eye has much shorter photoreceptors and its structure and function are more sensitive to photoreceptor energy demands: photoreceptors length is greatly reduced by and information capacity decreases by as much as 90% (Figures 7, 8). We conclude that when apposition and simple eyes are designed to use resources efficiently, the cost of the photoreceptor array is as significant as the cost of optics, and matching investments in optics and photoreceptor arrays to increase efficiency is a principle of eye design. Our analysis, which is the first to account for the costs of both optics and photoreceptor array, indicates that one benefit of investing in an eye, the ability to gather more information follows the law of diminishing returns. As expected from its superior geometry (Kirschfeld, 1976), a simple eye is in theory a better investment: its information capacity increases as (total cost)$^{0.8}$, compared with (total cost)$^{0.55}$ for an apposition eye, and the simple eye is 10 to 100 times more efficient at gathering information (Figure 8). We now discuss the validity of our methodology, the robustness of our findings, and their contributions to our understanding of eye design and evolution.

Specific volume is a useful measure of cost

This new measure of cost has several advantages. First, specific volume is defined by dimensions and angles that are measured anatomically and optically (Equations 1, 2, 5, 6) and relates directly to benefits via optical, geometrical and physiological constraints on spatial acuity and sensitivity. Thus, like previous indicators of cost - eye radius, eye length, pupil area and corneal area (Brandon et al., 2015; Brandon & Dudycha, 2014; Snyder et al., 1977; K. N. Thomas et al., 2020; R. J. Thomas et al., 2004) - specific volume can evaluate investments and trade-offs that adapt eyes for specific purposes. Second, specific volume is more flexible and far reaching than previous indicators of cost because it can be applied to eyes that are not well approximated by solid spheres. Third, it applies to small eye regions. Fourth, it provides a common currency for comparing investments in different eyes, eye regions, and components within an eye (Figures 5, 6, 7). This facility enables one to investigate how and why resources are distributed across visual fields and, as we demonstrate here, evaluate trade-offs between investments in an eye's components. Given that biological processes and systems evolve to become more cost-efficient because costs depress fitness (Alexander, 1996; Niven & Laughlin, 2008; G. K. Taylor & Thomas, 2014), we suggest a fifth advantage: specific volume will help us understand how eyes are adapted and evolve.

How well does specific volume represent costs? Volume accurately measures one limiting resource, space, but because there are insufficient data, we have to make assumptions to calculate the costs of energy and materials. Assuming that the densities of an eye's cells, extracellular materials and fluid-filled cavities are close to 1, space is a reasonable proxy for three costs that increase in proportion to mass: the energy expended carrying an eye (carriage cost), materials, and cellular energy consumption (Witter & Cuthill, 1993).

Equating mass and carriage cost is a reasonable starting point. Experiments on individual animals - a human walker carrying a backpack (Bastien et al., 2005), a flightless ant carrying nectar (Duncan & Lighton, 1994), and a flying beetle carrying a heavy weapon (Goyens et al., 2015) - show that the cost of carrying an additional load is the load's mass times the individual's mass specific metabolic rate when moving unloaded.

Turning to the costs of the materials and energy used within the eye, there is no data for an apposition eye's dioptric apparatus. Nonetheless, its corneal lenses, pigment cells, and cones cells are densely packed with macromolecules, and because their optical function is passive (they refract and absorb) they contain very few, if any, mitochondria. Indeed, the corneal cuticle and the fluid filled pseudo-cone of fly NS eye are extracellular (Hardie, 1985). Thus, the assumption that the costs of materials and energy for the dioptric apparatus increase in fixed proportion to volume is a reasonable starting point.

Cost estimates can be adjusted for situations in which costs per unit volume are not equal, as illustrated by our treatment of photoreceptor energy consumption. To support transduction the photoreceptor array has an exceptionally high metabolic rate (Laughlin et al., 1998; Niven et al., 2007; Pangršič et al., 2005). We account for this higher energy cost by using the animal's specific metabolic rate (power per unit mass and hence power per unit volume) to convert an array's power consumption into an equivalent volume (Methods). Photoreceptor ion pumps are the major consumers of energy and the smaller contribution of pigmented glia (Coles, 1989) is included

in our calculation of the energy tariff K_E (Methods). The higher costs of materials and their turnover in the photoreceptor array can be added to the energy tariff K_E but given the magnitude of the light-gated current (Laughlin et al., 1998) the relative increase will be very small. Thus, for our intents and purposes the effects of these additional costs are covered by our models. For want of sufficient data, K_E is uncertain, therefore we model a reasonable range of values (Methods). Because the optimum eye configuration is most sensitive to K_E in the lower half of this range (Figures 4, 7), we are unlikely to seriously underestimate the effects of photoreceptor costs on eye morphology and efficiency.

Matching photoreceptor length to spatial acuity

The systematic increase in rhabdomere or rhabdom length, L, with spatial acuity observed in apposition eyes (Figures 1, 5, 6) and simple eyes (see below), and predicted by our models (Figures 4, 7), is an obvious manifestation of efficient resource allocation. Two studies of apposition eyes, one of dragonfly and the other of praying mantis (Labhart & Nilsson, 1995; Rossel, 1979), map the covariation of lens diameter, D, interommatidial angle, $\Delta\phi$, and rhabdom length, L, across an entire eye. Both show that when acuity is increased by enlarging the dioptric apparatus and increasing ommatidial density, i.e. by reducing $\Delta\phi$, L is increased to improve SNR_{ph}. In both insects L peaks in a fovea that is used to detect and capture prey, and in dragonfly dorsal fovea the 1.1 mm rhabdomeres (the longest light sensitive waveguides reported in any eye, diurnal or nocturnal) are adapted to improve the detection and localisation of small flying prey (Labhart & Nilsson, 1995; Rigosi et al., 2017). However, specialisation for prey capture is unlikely to explain why L varies systematically with acuity across an entire eye.

We find that the trend to increase rhabdomere length with acuity is more generally advantageous. The trend is widespread: looking across 28 eye regions drawn from 10 species of fast flying insect, L increases with acuity over a 25-fold range of interommatidial angle (Figures 5, 6). Modelling shows that matching L to acuity improves a general measure of performance, spatial information capacity and the widespread covariation of L and acuity observed in apposition eyes follows the trend predicted by modelling (Figures 5, 6). Finally, because information capacity captures the interplay between three basic determinants of image quality, $\Delta\rho$, $\Delta\phi$ and SNR_{ph}, several tasks could benefit from an increase in L with acuity.

Other factors can link L to acuity. One possibility, developmental constraints impose inflexible scaling relationships on apposition eyes, can be dismissed. Scaling changes across apposition compound eyes (Perl & Niven, 2016; Scales & Butler, 2016; G. J. Taylor et al., 2019), and our empirical log-log plots of L v.s. eye volume and L v.s. D continuously change slope (Figure 5d,e), as required for the efficient allocation of resources (Figure 4c). Head size is an obvious constraint: smaller insects have smaller heads, consequently they will tend to have smaller eyes with lower acuity and shorter rhabdom(ere)s. The strongest evidence that lack of headroom reduces the length of photoreceptors comes from the fovea of a small insect, *Holcocephala* (Wardill et al., 2017), that is adapted for exceptionally high acuity (Table 2; Figure 5d). One must also consider the costs associated with enlarging the head by adding more eye, such as mechanical support, wind resistance, and conspicuousness. We suggest that more comparative studies are required to establish the influence of head

size on eye design.

Then there is the difference in L that is so obvious and widespread that it has been accepted without question - L is generally much longer in diurnal apposition eyes than in diurnal simple eyes. Comparing eyes with rhabdomeric photoreceptors, L ranges from 60 µm to 1100 µm in apposition eyes (Tables 2 & 3), and from 10 µm to 90 µm, in spiders' simple eyes (Land, 1985). Efficient resource allocation provides an explanation: optimised simple eye models predict that L is approximately x10 shorter than in apposition compound eyes of the same cost (Figure 7b). L also increases with acuity (increasing D and decreasing $\Delta\phi$) in optimised simple eye models and there is evidence that this matching occurs in diurnal spiders. L increases with increasing D when comparing eyes in different species (Land, 1985), different eyes in the same individual, and the same eye increasing in size and acuity as a juvenile spider grows to adulthood (Gote et al., 2019). However, more accurate models of these spiders' eyes are needed prove that this co-variation is increasing efficiency. The degree to which the lengthening of cone outer segments in primate fovea (Provis et al., 2013) increases the efficiency of resource utilisation is also an open question. A critical ingredient, a physiological constraint that links investments in outer segments to noise levels in full daylight, has yet to be identified in ciliary photoreceptors. In addition, the economics of vertebrate simple eyes differs from invertebrate simple eyes in two ways. First, a vertebrate outer segment is almost 10 times more effective at absorbing photons because its folded sheets of membrane pack visual pigment molecules more densely than arrays of tubes (microvilli) (Fain et al., 2010). Second, photoreceptors compete with neural circuits for resources within the eye (Kröger & Biehlmaier, 2009; Sterling & Laughlin, 2015).

Photoreceptor costs are a major factor in eye design

In apposition eye models optimised for spatio-temporal information capacity more than 40% of total investment, C_{tot}, is allocated to photoreceptor arrays (Figures 4e, 6e) and, in line with this theoretical finding, our analysis of data from diurnal insects shows that arrays occupy 30% to 75% of eye volume (Figures 5f, 6d). For simple eye models the efficient allocation is 30% to 60% of C_{tot} (Figure 7d). Our modelling identifies roles for two types of array cost, the rarely considered costs associated with array volume (Baden & Nilsson, 2022; Kirschfeld, 1976; Kröger & Biehlmaier, 2009), and the well-known energy costs associated with phototransduction (Ames, 2000; Fain & Sampath, 2021; Laughlin et al., 1998; Okawa et al., 2008; Pangršič et al., 2005). We find that this energy cost greatly influences the configuration of an efficient eye: increasing the energy tariff K_E reduces array depth, L, as much as tenfold (Figures 4c, 5d, 6c, 7b). Reducing L reduces SNR_{ph} (Equation 4), however the SNR_{ph} that remains is worth paying for because the $\%C_{tot}$ allocated to photoreceptor energy consumption increases (Figures 4f, 7e). We conclude that because SNR_{ph} is valuable, photoreceptor costs are always significant and this necessitates efficient resource allocation. It follows that photoreceptor costs influence the morphologies of both photoreceptor array and dioptric apparatus because optics and array compete for the resources invested in an eye.

The impact of photoreceptor costs depends on eye type

Photoreceptor energy cost has more impact on both the total cost and the design of a simple eye than an equivalent apposition compound eye because the simple eye has more photoreceptors per unit volume (Figure 7a). Applying our lowest energy tariff, K_E =0.04 µm^3 per microvillus, to an optimised apposition eye model has almost no effect on the depth of the photoreceptor array, L, but in the optimised simple eye model it reduces L by more than 80%, and array volume by more than 60% (Figure 7c). Despite this shrinkage, investment in the simple eye model's photoreceptor array increases from 35% C_{tot} to 50% C_{tot} because energy costs have risen from 30% C_{tot} to 55% C_{tot} (Figure 7d). Also, in simple eye models the percentages of C_{tot} allocated to the photoreceptor array volume and energy change very little as C_{tot} increases, whereas in apposition eyes the relative contribution of photoreceptor energy consumption falls steeply as photoreceptors become increasingly widely spaced (Figure 7a). Thus the distribution of costs within an efficiently configured eye changes with eye type, according to the eye's typical geometry .

Efficiency depends on eye type and photoreceptor energy cost

In both apposition and simple eye models, efficiency decreases with increasing C_{tot} (Figure 8b), making a bit of information more expensive in a larger eye. The decline in efficiency with increasing eye size is steeper in apposition models, as expected from the well-known scaling relationships enforced by lens diffraction and eye geometry, spatial resolution increases as eye radius, R, in a simple eye and as $\sqrt{R}$ in an apposition eye (Kirschfeld, 1976). However, using R as a measure of investment fails to identify the contribution of the photoreceptor array and fails to account for the fact that an apposition eye is not a solid sphere. When our more realistic measure of cost, specific volume, is used a *Drosophila* size apposition eye is 10 times less efficient than a simple eye of the same cost and a dragonfly size eye is 100 times less efficient (Figure 8b). In both simple and apposition eyes efficiency is reduced by increasing the photoreceptor energy tariff K_E. This effect is much greater in simple eyes (Figure 8b) thus, as also found for the reduction of photoreceptor length (Figure 7b), K_E has more impact on the design of simple eyes.

Expanding our understanding of apposition eye design

We build on theoretical studies that show how constraints imposed by apposition optics, eye geometry and eye size determine spatial resolution and information capacity when eye radius R, and hence corneal area, represent the limiting resource (Howard & Snyder, 1983; Kirschfeld, 1976; Snyder et al., 1977). Howard & Snyder (1983) introduced the physiological constraint, transduction unit saturation, and showed that it increases the optimum value of eye parameter, p, in bright light by placing a fixed ceiling on SNR_{ph} that is equivalent to operating at a lower light level. We extend Howard and Snyder's (1983) approach by using a measure of cost, specific volume, that allows eye radius R to vary while total cost remains constant. This added realism allows us to raise and lower the SNR ceiling imposed by transduction units by trading investments in rhabdomere length against investments in dioptric apparatus. In so doing we discover that it is advantageous for photoreceptors to lengthen rhabdomeres so as to reduce shot noise. Indeed, in daylight

Calliphora vicina R1-6 achieve the lowest level of photoreceptor noise reported to date, an equivalent contrast of 0.0084 (Anderson & Laughlin, 2000). This extreme specialisation resembles Autrum's proposition that apposition eye photoreceptors compensate for poor spatial resolution by increasing temporal resolution (Autrum, 1958), thereby achieving the highest flicker fusion frequencies known, in excess of 400 Hz (Tatler et al., 2000). Perhaps enhancing photoreceptor performance to compensate for optical inefficiency is a principle of apposition eye design?

Increasing temporal resolution increases photoreceptor energy consumption, so to improve efficiency apposition eye photoreceptors match temporal bandwidth to the properties of the images they form (Laughlin & Weckström, 1993; Niven et al., 2007). Eye regions that have lower spatial resolution and encounter more slowly moving images save energy by reducing photoreceptor bandwidth (B. G. Burton et al., 2001). Although this matching makes large energy savings it is not included in our models because, to reduce the burden of establishing proof of principle, we fix photoreceptor bandwidth at the high value measured in a fully light-adapted blowfly. Nonetheless, our models can accommodate the costs and benefits of changing temporal bandwidth because they operate in the frequency domain (Methods). Boosting temporal resolution will be more cost-effective in large apposition eyes because photoreceptor energy costs are marginalised by costs associated with array volume (Figure 4e,f), therefore investments of energy that increase temporal bandwidth are increasing the return on the much larger investment in array volume (e.g. carriage cost). Some fast flying diurnal insects with large facet lenses reduce the carriage cost of the photoreceptor array by surrounding each ommatidium with a palisade of air-filled tracheae (Horridge, 1969; Laughlin & McGinness, 1978; Smith & Butler, 1991; Wardill et al., 2017). The volumes and savings involved can be large. Published micrographs of dragonfly dorsal eye (Horridge, 1969) suggest that air fills at least 50% of array cross section.

How efficiently do insects allocate resources within their apposition eyes?

In principle one can establish the efficiency of an insect's investments in optics and photoreceptors by computing the performance surface for a model eye region that has the same parameters as the insect's eye region, then observing how closely the insect's eye region approaches the optimum configuration. We cannot do this at present because a critical parameter, the photoreceptor energy tariff K_E, has not been determined: the best we can do is use data from blowflies to estimate K_E's likely range (Methods). Not knowing K_E is a major impediment to obtaining exact fits of our models to data because our modelling has discovered that the morphology of an efficient eye is sensitive to photoreceptor energy costs: in apposition eyes, increasing K_E across its likely range reduces the depth of the photoreceptor array by as much as 90% (Figure 4c). Nor can we use our models to infer K_E by adjusting it to fit the data. Changing K_E has very little effect on D and $\Delta\phi$, therefore we must fit the model to L, and this requires several data points from eyes of the same species because K_E will be species specific (Methods). In our most consistent data set, the NS eyes (Figure 5; Table 2), it is impossible to obtain a satisfactory fit: the 12 data points come from 7 species and there are never more than 2 points per species. There are several data points per species for fused rhabdom apposition

eyes (Figure 6; Table 3), but in each of the four species the data points are too widely scattered to obtain a useful fit. This scatter in values of L is not surprising. Our generic fused rhabdom model glosses over the large differences in F-number and rhabdom diameter seen within the eye of each species (Table 3), and these differences probably reflect the specialisation of eye regions for different purposes, e.g. in the fovea the detection, tracking and interception of mates and prey, and in the periphery the monitoring of optic flow and the detection of potential prey and predators (Labhart & Nilsson, 1995; Menzel et al., 1991; Straw et al., 2006; van Hateren et al., 1989). This proposition is supported by the observation that the empirical data for D and $\Delta\phi$ (Figure 6a,b) are also more widely scattered than the data for the more homogeneous group, fly NS eyes (Figure 5a,b). Because our method calculates three basic determinants of the quality of the captured image, $\Delta\phi$, $\Delta\rho$ and SNR_{ph}, it can be adapted to compute performance surfaces for these specialised tasks, however the necessary theory has not been developed.

Having raised the question, efficient for what, we must examine our assumption that every eye region of a diurnal insect is adapted for vision in full daylight. The fact that insects in our data sets have larger lenses, interommatidial angles and eye parameters than our models predict (Figure 5) suggests that their eye regions are adapted for lower light levels (Snyder, 1979). We can think of two mutually inclusive reasons why a diurnal eye will not be adapted for vision in full daylight. The eye might be adapted for the time of day when the behaviour it supports is most profitable, e.g. insects that are most active early and/or late in the day to avoid predators and desiccation, and insects that prey on these crepuscular insects. Second, because an eye's performance surface is flat-topped, an eye region optimized for an intermediate light intensity might, when averaged over the daylight hours, perform better than an eye adapted for bright light. Our models can be developed to investigate how costs and benefits influence the design of eyes adapted for lower light levels (see below), and modified to investigate two further reasons for increasing the eye parameter p, higher image speeds (Snyder, 1979) and increasing D in "bright zones" to improve the detection of small targets and small movements (Straw et al., 2006; van Hateren et al., 1989)

In summary, for want of both data and theory, we are currently unable to quantify the efficiency with which an apposition eye region performs the function for which it is adapted. Nonetheless, we have two reasons to conclude that flying diurnal insects allocate resources to the optics and photoreceptor arrays of their apposition eyes efficiently. First, the empirical values we extract from published data lie within or close to the boundaries defined by our theoretical curves for eyes that maximise a general-purpose measure of performance, information capacity (Figures 5,6). Second, the flat-topped performance surfaces have extensive high-efficiency zones within which an eye's morphology can be changed while retaining >95% of the maximum information capacity (Figure 3). Thus eyes that are not optimised to maximise information capacity can still be gathering information with high efficiency. This observation speaks to the value of deriving performance surfaces: one can consider competing demands, evaluate loss of function and identify compromises.

Efficient resource allocation is a general principle

Efficient resource allocation is observed at many levels of biological organization, from single molecules to life histories (Bigman & Levy, 2020; Garland et al., 2022; Nijhout & Emlen, 1998; Stearns, 1989). Eyes are no exception. In an apposition eye, optical radius, R, represents corneal surface area per unit solid angle, therefore models that maximise spatial acuity or information capacity at constant R show that corneal area can be allocated to facet lenses to maximise spatial acuity and information capacity by trading spatial resolution for SNR (Snyder, 1977; Snyder et al., 1977). In the POL region of fly NS eye a fixed resource, the number of microvilli in the central rhabdom, is allocated to a pair of photoreceptors, R7 and R8, to increase the efficiency of polarisation coding (Heras & Laughlin, 2017), and in primate eye retinal area is allocated to cone spectral types to increase coding efficiency (Garrigan et al., 2010; Zhang et al., 2022).

Matching the sampling density of the photoreceptor array to lens resolving power (Nilsson & Land, 2012) also allocates the resources invested in photoreceptors more efficiently by avoiding wasteful overcapacity, according to the principle of symmorphosis (Piersma & van Gils, 2011; C. Taylor & Weibel, 1981; Weibel, 2000). However, unlike the matching of L to $\Delta\phi$ that allocates resources efficiently to optics and photoreceptors, the matching of capacities does not consider the individual cost-benefit functions of a system's components. When these are taken into account, the allocation of investment that maximises efficiency can instal over-capacity in components with more favourable cost-benefit ratios, as demonstrated for bones in racehorse forelegs (Alexander, 1997) and chains of signalling molecules (Schreiber et al., 2002).

Understanding the adaptive radiation of eyes

The method we introduce here can be developed to view several aspects of eye adaptation and evolution through a cost-benefit lens because it is flexible. Our approach is not wedded to information capacity: it supports other measures of visual performance because it relates investments to fundamental determinants of image quality. Moreover, the method can be applied to several trade-offs that influence eye design by relaxing the simplifying assumptions we make here. To give a concrete example, the trade-offs between acuity and sensitivity that adapt eyes for nocturnal or diurnal vision can be viewed through a cost-benefit lens by allowing F-number and rhabdom(ere) diameter to vary, and by adopting a method that calculates the mean and variance of photon transduction rate on N_{vil} in rhabdomeres of any given length and variable cross section, at any biologically plausible light intensity (Heras & Laughlin, 2017).

One can also relax the restrictions we place on eye geometry. Our approach does not depend on spherical geometry, it depends on being able to relate the shapes, sizes and constituents of an eye's components to their costs and performance. Advances in scanning, imaging and digital reconstruction offer opportunities to determine shapes, volumes and constituents directly, and advances in modelling optical and physiological processes are extending our ability to relate these properties to performance (Kim, 2014; Song et al., 2012; Sumner-Rooney et al., 2019; G. J. Taylor et al., 2019). These powerful new methods can take us closer to the goal of understanding of how costs, benefits and innovative mechanisms drive eye evolution

(Sumner-Rooney, 2018), and our flexible cost-benefit approach can support this endeavour.

Our approach also identifies factors that contribute to selective pressure, and gauges their effects. For example, the pressure to reduce photoreceptor energy cost depends on a photoreceptor's impact on an animal's energy budget. This effect is captured by our photoreceptor energy tariff, K_E, because it relates a photoreceptor's energy consumption to the animal's metabolic rate (Methods). We also find that photoreceptor energy costs are marginalised when apposition eye size increases and this encourages the use of wide bandwidth, high *SNR* photoreceptors with high metabolic rates. Most interestingly, the derivation of performance surfaces (Figure 3) reveals a large area, the robust high-performance zone within which an eye's morphology can be adapted to a particular task while retaining more than 95% of a measure of general-purpose capability, information capacity. This low "loss of opportunity" cost helps to explain the remarkable degree of fine tuning observed in apposition compound eyes (B. G. Burton et al., 2001; Land, 1997; Nilsson & Land, 2012; Sumner-Rooney et al., 2019; G. J. Taylor et al., 2019), in line with suggestions that robustness increases evolvability (Drack & Betz, 2022).

Two key steps in the early evolution of eyes were the stacking of photoreceptive membranes to absorb more photons, and the formation of optics to intercept more photons and concentrate them according to angle of incidence (Nilsson, 2013, 2021). Our modelling of well-developed image forming eyes shows that to improve performance stacked membranes (rhabdomeres) compete with optics for the resources invested in an eye, and this competition profoundly influences both form and function. Thus it is likely that competition between optics and photoreceptors was shaping eyes as lenses evolved to support low resolution spatial vision. If so, the developmental mechanisms that allocate resources within extant high resolution eyes (Casares & McGregor, 2021), by controlling cell size and shape and, as our study emphasises, setting up gradients of shape and size across the eye, will have analogues or homologues in ancient eyes. Their discovery will not only tell us how Nature constructs perfectly contrived instruments, it will illuminate the evolutionary pathway to perfection.

Methods

Calculating a photoreceptor array's information rate

Our calculations of the rate at which an eye's photoreceptor array codes achromatic information, in bits per steradian per second, take account of five factors. 1) The statistics of the signals presented to an eye under natural conditions; 2) the blurring of the spatial image by the eye's dioptric apparatus; 3) the sampling of the spatial image by the photoreceptor array; 4) the introduction of noise by the stochastic activation of a finite population of transduction units and 5) the temporal smoothing of signals and noise during phototransduction. We calculate information rates in the frequency domain using methods developed for apposition eyes (de Ruyter van Steveninck & Laughlin, 1996; Howard & Snyder, 1983; Snyder et al., 1977; van Hateren, 1992).

Natural intensity signals

We calculate the spatial and temporal power spectra of naturalistic signals using the model established for blowfly (van Hateren, 1992). An eye images an ensemble of natural scenes in which power decreases as the square of spatial frequency, as measured and predicted theoretically (G. J. Burton & Moorhead, 1987; Ruderman, 1997; van Hateren, 1992). Consequently the two dimensional power spectrum of the spatial frequencies viewed by the eye is

$$S_{xy} = \frac{c_c}{f_x^2 + f_y^2} \tag{12}$$

The proportionality constant c_c is chosen to set the total contrast of the image formed by the eye (defined as the square root of the ratio between the power of the signal and the square of the mean level of signal) to an appropriate value. This contrast depends on the eye that observes the scene. For images spatially filtered by a blowfly compound eye the average contrast, calculated locally over intervals of 25-50 degrees, is 0.4 (Laughlin, 1981). Accordingly we use a proportionality constant that scales the power of frequencies between one cycle per 50 degrees and the upper cut-off frequency dictated by sampling, one cycle per 1.5 degrees, to be $(0.4)^2 = 0.16$.

To add the temporal dimension van Hateren (1992) modelled how the movement of an eye through an ensemble of uniformly distributed objects generates temporal structure. For the case of an eye moving in a straight line, the structure is adequately described by a random distribution of angular speeds

$$a_v(v) = \frac{c_v}{(|v| + \sigma_v)^2} \tag{13}$$

where $a_v(v)$ is the probability of encountering image speed v, c_v is the normalization constant that sets the sum of probabilities over the distribution to 1, and σ_v is a constant that regulates the width of the distribution. Local movements produced by objects moving within a scene, although acknowledged to be biologically significant, have little impact on the statistics of the signal encountered by an eye moving in a straight line (van Hateren, 1992).

Distributions of this form peak at lower speeds and have a long tail that extends to speeds faster than σ_v. The exact value of σ_v will depend on the behaviour of the animal. For *Calliphora vicina* yaw, pitch and roll movements rarely exceed $3.5\,\mathrm{rad\,s^{-1}}$ between saccades (van Hateren & Schilstra, 1999). Assuming a similar limit in translational movements, we take σ_v to be $1\,\mathrm{rad\,s^{-1}}$. In his earlier 1992 paper van Hateren assumed σ_v is $0.29\,\mathrm{rad\,s^{-1}}$ and noted that the information capacities he calculated are not particularly sensitive to σ_v.

The three-dimensional power density of naturalistic signals generated by the aforementioned distributions is

$$S_{xyt}(f_x, f_y, f_t) = \frac{\pi}{2f_r^3} c_c a_v \left(\frac{\pi}{2}\frac{f_t}{f_r}\right) \tag{14}$$

where $f_r = \sqrt{f_x^2 + f_y^2}$ and c_c is the proportionality constant used in Equation 12. We checked that this distribution retains the local contrast value of 0.4 for different values of the parameter $|\sigma_v|$.

Blurring by the optics

The lens point spread function and the angular sensitivity of the photoreceptor entrance aperture combine to determine photoreceptor angular sensitivity, which in the eyes we consider approximates a Gaussian function of half-width $\Delta\rho$. The transfer function of this spatial filter is

$$m(f_x, f_y) = \exp\left(-\frac{\pi^2}{4\ln 2}(f_x^2 + f_y^2)\Delta\rho^2\right) \tag{15}$$

The lens is diffraction limited and the photoreceptive rhabdomeres and rhabdoms are waveguides, consequently calculating the acceptance angle of this coupled system is a complicated problems of wave optics, especially when, with narrow d_{rh}, waveguide effects are significant (Stavenga, 2003a, 2003b, 2004a, 2004b). We employ two expressions for photoreceptor acceptance angle. One is Snyder's (1979) convolution of Gaussians (CoG) approximation

$$\Delta\rho^2 = (\lambda/D)^2 + \Delta\rho_r^2 \tag{16}$$

where λ is the wavelength of light, D is lens diameter, λ/D is the half-width of the Airey disk and $\Delta\rho_r$ is the angular acceptance of the rhabdomere, taken to be its angular subtense, $\Delta\rho_r = d_{rh}/f$.

The other is Stavenga's more principled expression, obtained using his wave optics model (WOM) of larger fly NS eyes (Stavenga, 2004a)

$$\Delta\rho = 1.26\lambda/D \tag{17}$$

Stavenga's WOM shows that the coefficient in Equation 17 reduces progressively as the fly's longitudinal pupil closes, reaching a minimum of 1.14 when fully closed in full daylight. We use an intermediate value, 1.26, because the pupil closes progressively over the upper two log units of daylight intensity, while holding SNR_{ph} close to maximum.

Temporal filtering during phototransduction

A photoreceptor's elementary response to a single photon, a quantum bump, is generally fitted with functions of the type

$$h(t) \propto \left(\frac{t}{\tau}\right)^{\alpha-1} e^{-t/\tau} \tag{18}$$

whose Fourier transform is

$$H(f) = \frac{1}{(1 + i2\pi\tau f)^\alpha} \tag{19}$$

Thus transduction's first temporal low pass filter has the form

$$|m_t(f_t)|^2 = \frac{1}{(1 + (2\pi\tau f)^2)^\alpha} \tag{20}$$

We use the fit of $\alpha = 3.12$ measured in *Musca* (B. G. Burton, 2006) and $\tau = 0.001\,\mathrm{s}$ obtained in *Calliphora* at the highest light intensities (Juusola et al., 1994).

According to these values photon shot noise power falls to half-maximum at around 170 Hz.

Following the activation of a microvillus by an absorbed photon the quantum bump is produced with a variable delay. This latency dispersion low-pass filters signals that are composed of many bumps by widening the impulse response. We use the low-pass filter

$$|m_d(f_t)|^2 = \frac{1}{(1 + (2\pi\tau_d f)^2)^{\alpha_d}} \tag{21}$$

where $\alpha_d = 2$ (Wong et al., 1980). With $\tau_d = 0.0014\,\mathrm{s}$ this filter produces a signal corner frequency close to the 55 Hz measured in *Calliphora vicina* (Anderson & Laughlin, 2000). The trends we observe in our study are not critically dependent on the exact values of these bump parameters.

Sampling

For one dimensional receptor arrays, frequencies will not be correctly sampled above the Nyquist limit (Snyder, 1979)

$$f_{Ny} = \frac{1}{2\Delta\phi} \tag{22}$$

where ϕ, as defined above, is the sampling angle of the array.

For a two dimensional hexagonal lattice, only frequencies up to $\frac{1}{\sqrt{3}\Delta\phi}$ can be sampled independently of the orientation of the array (Snyder et al., 1977). These authors also noted that frequencies up to $\frac{1}{\Delta\phi}$ can be sampled for special orientations of the array, however we will assume that the highest spatial frequencies sampled by an array is $\frac{1}{\sqrt{3}\Delta\phi}$.

Deriving the signal coded by the array

To obtain the power spectral density of the signal coded by a photoreceptor the natural image signal derived above is spatially filtered by the dioptric apparatus, converted to a stream of shot events, quantum bumps, with mean rate ψ, and temporally filtered during phototransduction. We start with van Hateren's (1992) expression for the signal coded by a photoreceptor that is transducing photons at a rate ψ

$$(\Delta S)^2 (f_x, f_y, f_t) = \psi^2 S_{xyt}(f_x, f_y, f_t)|m(f_x, f_y)|^2|m_t(f_t)|^2|m_d(f_t)|^2 \tag{23}$$

This expression assumes that the photoreceptor signal increases linearly with photon capture rate, as happens at low light levels when the saturation of transduction units is negligible, and signal and noise follow Poisson statistics.

In brighter conditions the saturation of microvilli changes the relationship between transduction rate, ψ and photoreceptor signal ΔS (Howard et al., 1987). The probability that a microvillus generates a signal is given by

$$p = \frac{I}{N_{vil}/\tau_r + I} \tag{24}$$

where I, the effective intensity, is the rate at which microvilli are absorbing photons, and the cycling time τ_r is the average time taken to reset a microvillus to its receptive state, following activation by a photon capture (Howard et al., 1987).

The transduction rate is given by

$$\psi = pN_{vil}/\tau_r \tag{25}$$

There are some limits to this treatment. Because light intensity decreases along the rhabdom(ere), microvilli in the distal part will, in principle, absorb more photons than microvilli in the proximal part, making it impossible for all microvilli to have the same probability of being active. However, adaptations have been described that partially compensate for this effect by reducing the quantum capture efficiency of distal microvilli (Labhart & Nilsson, 1995).

According to the saturation equation (24), the light intensity that activates half the microvilli, $I_{50} = N_{vil}/\tau_r$. Therefore the dependence of transduction rate on I is given by

$$\psi = pN_{vil}/\tau_r = \frac{I_{50}I}{I_{50} + I} \tag{26}$$

and

$$\frac{d\psi}{dI} = \frac{I_{50}^2}{(I_{50} + I)^2} \tag{27}$$

$\Delta\psi$, the change in ψ produced by a change in intensity, ΔI, is given by

$$\Delta\psi = \frac{d\psi}{dI}\Delta I = \frac{d\psi}{dI}cI \tag{28}$$

where c is the stimulus contrast (Howard et al., 1987)

Under the condition we model, half-saturation of transduction units, $I = 2\psi$ and $\frac{d\psi}{dI} = \frac{1}{4}$. Consequently the photoreceptor signal is

$$(\Delta S)^2 (f_x, f_y, f_t) = \left(\frac{\psi}{2}\right)^2 S_{xyt}(f_x, f_y, f_t)|m(f_x, f_y)|^2|m_t(f_t)|^2|m_d(f_t)|^2 \tag{29}$$

where

$$\psi = \frac{N_{vil}}{2\tau_r} \tag{30}$$

In the fly NS eye 6 photoreceptors sample the same point in space, therefore the signal transmitted for each pixel in the array is

$$(\Delta S)^2 (f_x, f_y, f_t) = (3\psi)^2 S_{xyt}(f_x, f_y, f_t)|m(f_x, f_y)|^2|m_t(f_t)|^2|m_d(f_t)|^2 \tag{31}$$

Noise

We consider shot noise generated at the first step in the generation of a quantum bump, the absorption of a photon by a rhodopsin molecule in a microvillus that is not currently processing a bump. Noise generated elsewhere in photoreceptors is not incorporated in our model. Assuming that the photon capture rate ψ is never far from its average value, the shot noise power in a single photoreceptor is given by:

$$\sigma_{sn}^2(f_t) = \frac{\psi}{2}|H(f_t)|^2 \tag{32}$$

where $|H(f_t)|$ is the Fourier transform of the quantum bump and the factor 2 takes account of the fact that at half-saturation the statistics of microvillus activation are binomial (Howard et al., 1987).

Substituting from Equation 20

$$\sigma_{sn}^2(f_t) = \frac{\psi}{2}|m_t(f_t)|^2 \tag{33}$$

We assume that the shot noise in different photoreceptors is uncorrelated, therefore the shot noise generated by the 6 photoreceptors coding a pixel is

$$\sigma_{sn}^2(f_t) = 3\psi|m_t(f_t)|^2 \tag{34}$$

Because we assume that the shot noise in different photoreceptors is uncorrelated the power spectrum of shot noise, is on average, the same across the photoreceptor array

$$\sigma_{sn}^2(f_x, f_y, f_t) \propto \begin{cases} 3\psi|H(f_t)|^2 & \text{if } (f_x, f_y) \text{ is sampled} \\ 0 & \text{if } (f_x, f_y) \text{ is not sampled} \end{cases} \tag{35}$$

with the proportionality constant being the inverse of the area in frequency space that is sampled by the photoreceptor array.

Aliasing

When the image projected to the photoreceptor array contains spatial frequencies that are beyond the spatial resolving power of the array, these are aliased to lower frequencies, thereby distorting the sampled image (Snyder et al., 1994). We assume that all aliased spatial frequencies act as noise, shared equally between the correctly sampled spatial frequencies:

$$\sigma_{al}^2(f_t) = \psi^2 k(f_t) \tag{36}$$

Calculating Information

We calculate the spatial information gathered by the photoreceptor array by modifying the formula for a square spatial sampling lattice (Howard & Snyder, 1983). For a hexagonal array, the equation for spatial information has the form

$$H = A\int_0^{\mu_s} f_r \log_2[1 + (S/N)(f_r)]df_r \tag{37}$$

where the array cut-off frequency is $\mu_s = \frac{1}{\sqrt{3}\Delta\phi}$. To obtain the factor A, we consider the extreme case where the signal-to-noise ratio is constant across all spatial frequencies, in which case

$$H = A\frac{1}{3(\Delta\phi)^2}\log_2[(N_i)] \tag{38}$$

where $N_i = \sqrt{1 + S/N}$ is the number of discriminable levels of contrast coded by each ommatidium. The factor multiplying $\log_2[N_i]$ is the number of ommatidia in a steradian, which for a hexagonal lattice is $1/S_{\hexagon} = \frac{2\sqrt{3}}{3(\Delta\phi)^2}$. Thus $A = 2\sqrt{3}$. Therefore spatial information capacity per steradian is

$$H = 2\sqrt{3}\int_0^{\mu_s} f_r \log_2[1 + (S/N)(f_r)]df_r \tag{39}$$

We then extend this equation for spatial information capacity to the temporal domain (van Hateren, 1992). For a spatio-temporal signal the information capacity is

$$H = 2\sqrt{3}\int_{-\infty}^{\infty}\int_{0}^{\mu_s} f_r \log_2[1 + (S/N)(f_r, f_t)]df_t df_r \tag{40}$$

Inserting signal and noise

$$H = 2\sqrt{3}\int_{-\infty}^{\infty}\int_{0}^{\mu_s} f_r \log_2(1 + \frac{(\Delta S)^2 (f_r, f_t)}{\sigma_{sn}^2(f_r, f_t) + \sigma_{al}^2(f_t)})df_t df_r \tag{41}$$

Ballpark estimate of the photoreceptor energy tariff

Energy consumed per microvillus

Our estimates are based on high resolution measurements of the oxygen consumed by isolated *Calliphora vicina* compound eyes, made using a magnetic diver balance (Pangršič et al., 2005). In bright light, an eye consumes 1.8×10^{-9} litres of oxygen per second which, converting to the units commonly used to express metabolic rates, is 6.48 mm^3 of oxygen per hour. With 5000 ommatidia, 60,000 microvilli in the rhabdomere of a photoreceptor R1-6, and taking the central rhabdom formed by R7 and R7 to be equivalent to a single R1-6, the eye contains 2×10^9 microvilli, giving an oxygen consumption per microvillus in bright light $O_{vil}^L = 3.24\times10^{-9}$ mm^3 oxygen per microvillus per hour. In darkness the eye's oxygen consumption drops to one third, giving $O_{vil}^D = 1.08 \times 10^{-9}$ mm^3 oxygen per microvillus per hour.

Because these estimates are based on measurements from whole eyes they include consumption by all cell types. There are three reasons why photoreceptors dominate total consumption. First, the values of an eye's oxygen consumption in light and in darkness are close to the total photoreceptor consumption predicted from electrophysiological estimates of the ATP consumed by single photoreceptors (Laughlin et al., 1998; Pangršič et al., 2005). Second, photoreceptors are the compound eye's most active cells because transducing photons at high light intensities necessarily requires large fluxes of ions and chemical intermediates. Third, to support their activity photoreceptors contain most of a compound eye's mitochondria.

The rate of oxygen consumption averaged over the course of 24 hrs $\bar{O}_{vil}$, depends on the hours of daylight, DL

$$\bar{O}_{vil} = \frac{DL * O_{vil}^L + (24 - DL) * O_{vil}^D}{24} \text{ mm}^3 \text{ oxygen per mg per hour} \tag{42}$$

Energy consumed by the fly

To convert the energy consumption of the eye per microvillus into an equivalent volume we should ideally use the animal's average specific metabolic rate, measured under natural conditions, but to the best of our knowledge this field metabolic rate has not been measured in blowflies. Therefore, we combine a value of the specific metabolic rate in continuous flight that is towards the high end of the range measured in *Calliphora*, $sFMR = 30$ mm^3 oxygen per mg per hour (Yurkiewicz & Smyth, 1966), with the resting metabolic rate measured in the blowfly *Phormia*, $RMR = 2.6$ mm^3 oxygen per mg per hour (Keister & Buck, 1961; Niven & Scharlemann, 2005),

according the number of hours per day spent flying, T_F, to estimate the daily average specific metabolic rate

$$\overline{SMR} = \frac{T_F * sFMR + (24 - T_F) * RMR}{24} \text{ mm}^3 \text{ oxygen per mg per hour.} \quad (43)$$

Estimating the energy tariff, K_E

Assuming that the density of the eye is 1

$$K_E = \frac{\bar{O}_{vil}}{\overline{SMR}} \text{ mm}^3 \text{ of eye per microvillus} \quad (44)$$

To obtain a plausible range of values we calculate K_E in four conditions (Table 4)

T_F hrs	D_L hrs	K_E µm^3/microvillus
12	12	0.13
12	16	0.15
2	12	0.44
2	16	0.52

Table 3: Dependence of energy surcharge K_E on time spent flying T_F and hours of daylight D_L, calculated for blowfly

.

Note that, as expected, our measure of the impact of photoreceptor energy costs, K_E, depends on both the energy consumption per microvillus and the animal's metabolic rate: K_E is increased by increasing daily consumption by photoreceptors and decreased by increasing the animal's overall metabolic rate by increasing time flying, T_F.

Preliminary model of a simple eye

Our generic simple eye model has the same F-number $F = 2$ as our generic fly NS model, and its rhabdom diameter equals the rhabdomere diameter in in fly $d_{rh} = 1.9\,\mu\text{m}$. The simple eye is hemispherical (Figure 7a), therefore the specific volume of optics is given by

$$V_o = \frac{\pi}{3} f^3 = \frac{\pi}{3}(DF)^3 \mu m^3 sr^{-1} \quad (45)$$

and with a photoreceptor array with rhabdoms of length L, the total specific volume of the eye is given by

$$V_{tot} = \frac{\pi}{3}(DF + L)^3 \quad (46)$$

and the specific volume of the photoreceptor array by

$$V_{ph} = V_{tot} - V_o \quad (47)$$

The receptor spacing, $\Delta\phi$, depends on the lens focal length, f and d_{rh},

$$\Delta\phi = \frac{d_{rh}}{f} = \frac{d_{rh}}{DF} \quad (48)$$

This is an important difference between simple eyes and apposition eyes. In apposition eyes model $\Delta\phi$ is can be varied at constant f and D by changing the optical radius R. However, in a simple eye with a diffraction limited lens the relationship between the optical resolving power of the lens and the anatomical resolving power of the photoreceptor mosaic depends on F-number, F, as follows (Snyder, 1979). For a hexagonal mosaic of photoreceptors the diffraction limit is reached when

$$\lambda/D = \sqrt{3}\frac{d_{rh}}{f} = \sqrt{3}\frac{d_{rh}}{DF} \tag{49}$$

When λ, the wavelength of light is 500 nm, and $d_{rh} = 2\,\mu\text{m}$, then $F = 6.9$. It follows that our model simple eye with $F = 2$ is undersampling by a factor of approximately 3.5. Running our simple eye model with $F = 4$ had very little effect on the optimum L (data not shown), suggesting that our conclusion that efficient simple eyes have much shorter rhabdoms than efficient apposition eyes is robust with respect to undersampling.

Calculating N_{vil} as a function of L

We estimate v, the number of microvilli per unit length of rhabdomere, for our NS eye model using findings from photorevceptors R1-6 in female blowflies. Dividing the number of microvilli in a rhabdomere, 6×10^4 (Howard et al., 1987), by $L = 260\,\mu\text{m}$, which is towards the upper end of the range $L = 220\,\mu\text{m}$ - $280\,\mu\text{m}$ reported for blowfly (Hardie, 1985), gives $v = 230\,\mu\text{m}^{-1}$. Although fly rhabdomeres vary in both diameter and degree of taper according to eye region, sex and species, and this sculpting adapts photoreceptor arrays to visual ecology, e.g.(Gonzalez-Bellido et al., 2011), we fix v to simplify the derivation of points of principle.

For our generic model of a fused rhabdom apposition eye we consider a column of six photoreceptors that, like the short visual fibres R1-6 in fly, terminate in the first optic neuropile. Their six rhabdomeres form the triradiate rhabdom described in locust (Wilson et al., 1978). This fused rhabdom has a cross-section that approximates an equilateral triangle in which each side is constructed by a pair photoreceptors whose parallel microvilli are equivalent to a single fly R1-6 rhabdomere. Thus each pixel is coded by a set of six rhabdomeres that are equivalent to three fly R1-6 rhabdomeres. Therefore, the number of transduction units coding a pixel is half that in fly and the resulting changes in signal and noise are simply accounted for by replacing the factor $(3\psi)^2$ in Equation 29 with $\left(\frac{3\psi}{2}\right)^2$, and 3ψ in Equations 33 and 34 with $\left(\frac{3\psi}{2}\right)$.

For our generic model of a diurnal simple eye we assume that, as in spiders, the rhabdomeres of adjacent photoreceptors abut; i.e. there are no gaps between photoreceptors, therefore a photoreceptor's rhabdomeres project from a central column of cytoplasm. To compare with our apposition models we assume that the diameter of the photoreceptor entrance aperture, $d_{rh} = 1.9\,\mu\text{m}$ and contains microvilli projecting in three directions. In this case, the simple eye photoreceptor is equivalent to the triradiate fused rhabdom.

Authors' contributions

FJHH and SBL conceived of the project, FJHH developed, constructed, programmed and ran the models, FJHH and SBL applied the models, curated and analysed published data, and wrote the paper. FJHH's contributions were made while he was a member of the University of Cambridge.

Acknowledgements

We are grateful to Doekele Stavenga for his expert advice on optics, to Jeremy Niven for his advice during the project and his comments on the manuscript, and to Daniel Osorio and James Herbert-Read for their comments on the manuscript.

Funding

Francisco Heras was supported by a La Caixa Postgraduate Scholarship and a Caja-Madrid Postgraduate Scholarship. Simon Laughlin was supported by an honorarium from H. Britton Sanderford. The funders had no role in study design, data collection and analysis, the decision to publish, and the preparation of the manuscript.

References

Alexander, R. M. (1997). A theory of mixed chains applied to safety factors in biological systems. *Journal of Theoretical Biology*, *184*(3), 247–252. https://doi.org/10.1006/jtbi.1996.0270

Alexander, R. M. (1996). *Optima for animals*. Princeton University Press.

Ames, A. (2000). CNS energy metabolism as related to function. *Brain Research Reviews*, *34*(1), 42–68. https://doi.org/10.1016/S0165-0173(00)00038-2

Anderson, J. C., & Laughlin, S. B. (2000). Photoreceptor performance and the coordination of achromatic and chromatic inputs in the fly visual system. *Vision Research*, *40*(1), 13–31. https://doi.org/10.1016/S0042-6989(99)00171-6

Autrum, H. (1958). Electrophysiological analysis of the visual systems in insects. *Experimental Cell Research, Supplement*, *5*, 426–439.

Baden, T., & Nilsson, D.-E. (2022). Is our retina really upside down? *Current Biology*, *32*(7), R300–R303. https://doi.org/10.1016/j.cub.2022.02.065

Barlow, H. B. (1952). The size of ommatidia in apposition eyes. *Journal of Experimental Biology*, *29*(4), 667–674.

Bastien, G. J., Willems, P. A., Schepens, B., & Heglund, N. C. (2005). Effect of load and speed on the energetic cost of human walking. *European Journal of Applied Physiology*, *94*(1), 76–83. https://doi.org/10.1007/s00421-004-1286-z

Bigman, L. S., & Levy, Y. (2020). Proteins: Molecules defined by their trade-offs. *Current Opinion in Structural Biology*, *60*, 50–56. https://doi.org/10.1016/j.sbi.2019.11.005

Brandon, C. S., James, T., & Dudycha, J. L. (2015). Selection on incremental variation of eye size in a wild population of *Daphnia*. *Journal of Evolutionary Biology*, *28*(11), 2112–2118. https://doi.org/10.1111/jeb.12711

Brandon, C. S., & Dudycha, J. L. (2014). Ecological constraints on sensory systems: Compound eye size in *Daphnia* is reduced by resource limitation. *Journal of Comparative Physiology A*, *200*(8), 749–758. https://doi.org/10.1007/s00359-014-0918-y

Burton, B. G. (2006). Adaptation of single photon responses in photoreceptors of the housefly, *Musca domestica*: A novel spectral analysis. *Vision Research*, *46*(5), 622–635. https://doi.org/10.1016/j.visres.2005.09.020

Burton, B. G., & Laughlin, S. B. (2003). Neural images of pursuit targets in the photoreceptor arrays of male and female houseflies *Musca domestica*. *Journal of Experimental Biology*, *206*(22), 3963–3977. https://doi.org/10.1242/jeb.00600

Burton, B. G., Tatler, B. W., & Laughlin, S. B. (2001). Variations in photoreceptor response dynamics across the fly retina. *Journal of Neurophysiology*, *86*(2), 950–960. https://doi.org/10.1152/jn.2001.86.2.950

Burton, G. J., & Moorhead, I. R. (1987). Color and spatial structure in natural scenes. *Applied Optics*, *26*(1), 157–170. https://doi.org/10.1364/AO.26.000157

Casares, F., & McGregor, A. P. (2021). The evolution and development of eye size in flies. *WIREs Developmental Biology*, *10*(2), e380. https://doi.org/10.1002/wdev.380

Coles, J. A. (1989). Functions of glial cells in the retina of the honeybee drone. *Glia*, *2*(1), 1–9. https://doi.org/10.1002/glia.440020102

Cronin, T. W., Johnsen, S., Marshall, N. J., & Warrant, E. J. (2014). *Visual ecology*. Princeton University Press.

Darwin, C. (1859). *The origin of species by means of natural selection* (1st edtn.). John Murray.

de Ruyter van Steveninck, R. R., & Laughlin, S. B. (1996). The rate of information transfer at graded-potential synapses. *Nature*, *379*(6566), 642–645. https://doi.org/10.1038/379642a0

Drack, M., & Betz, O. (2022). A technomorphic conceptualisation of biological 'constructions' and their evolution. *Vertebrate Zoology*, *72*, 839–855. https://doi.org/10.3897/vz.72.e86968

Duncan, F. D., & Lighton, J. R. B. (1994). The burden within: The energy cost of load carriage in the honeypot ant, *Myrmecocystus*. *Physiological Zoology*, *67*(1), 190–203. https://doi.org/10.1086/physzool.67.1.30163842

Fain, G. L., Hardie, R., & Laughlin, S. B. (2010). Phototransduction and the evolution of photoreceptors. *Current Biology*, *20*(3), R114–R124. https://doi.org/10.1016/j.cub.2009.12.006

Fain, G. L., & Sampath, A. P. (2021). Light responses of mammalian cones. *Pflügers Archiv - European Journal of Physiology*, *473*(9), 1555–1568. https://doi.org/10.1007/s00424-021-02551-0

Feller, K. D., Sharkey, C. R., McDuffee-Altekruse, A., Bracken-Grissom, H. D., Lord, N. P., Porter, M. L., & Schweikert, L. E. (2021). Surf and turf vision: Patterns and predictors of visual acuity in compound eye evolution. *Arthropod Structure and Development*, *60*, 101002. https://doi.org/10.1016/j.asd.2020.101002

Garland, T., Downs, C. J., & Ives, A. R. (2022). Trade-offs (and constraints) in organismal biology. *Physiological and Biochemical Zoology*, *95*(1), 82–112. https://doi.org/10.1086/717897

Garrigan, P., Ratliff, C. P., Klein, J. M., Sterling, P., Brainard, D. H., & Balasubramanian, V. (2010). Design of a trichromatic cone array. *PLOS Computational Biology*, *6*(2), e1000677. https://doi.org/10.1371/journal.pcbi.1000677

Gonzalez-Bellido, P. T., Wardill, T. J., & Juusola, M. (2011). Compound eyes and retinal information processing in miniature dipteran species match their specific ecological demands. *Proceedings of the National Academy of Sciences*, *108*(10), 4224–4229. https://doi.org/10.1073/pnas.1014438108

Gote, J. T., Butler, P. M., Zureka, D. B., Buschbeck, E. K., & Morehouse, N. (2019). Growing tiny eyes: How juvenile jumping spiders retain high visual performance in the face of size limitations and developmental constraints. *Vision Research*, *160*, 24–36. https://doi.org/10.1016/j.visres.2019.04.006

Goyens, J., Van Wassenbergh, S., Dirckx, J., & Aerts, P. (2015). Cost of flight and the evolution of stag beetle weaponry. *Journal of The Royal Society Interface*, *12*, 20150222. https://doi.org/10.1098/rsif.20150222

Hardie, R. C. (1985). Functional organization of the fly retina. In H. Autrum, D. Ottoson, E. R. Perl, R. F. Schmidt, H. Shimazu, & W. D. Willis (Eds.), *Progress in sensory physiology* (pp. 1–79, Vol. 5). Springer Berlin Heidelberg. https://doi.org/10.1007/978-3-642-70408-6_1

Hardie, R. C., & Postma, M. (2008). Phototransduction in microvillar photoreceptors of *Drosophila* and other invertebrates. In R. Masland & T. D. Albright (Eds.), *The senses, a comprehensive reference. volume 1, vision 1* (pp. 77–130). Academic Press.

Heras, F. J. H., & Laughlin, S. B. (2017). Optimizing the use of a sensor resource for opponent polarization coding. *PeerJ*, *5*, e2772. https://doi.org/10.7717/peerj.2772

Horridge, G. A. (1969). Unit studies on retina of dragonflies. *Zeitschrift Fur Vergleichende Physiologie*, *62*, 1–37. https://doi.org/10.1007/BF00298040

Howard, J., Blakeslee, B., & Laughlin, S. B. (1987). The intracellular pupil mechanism and photoreceptor signal:noise ratios in the fly *Lucilia cuprina*. *Proceedings of the Royal Society of London. Series B, Biological Sciences*, *231*(1265), 415–435. https://doi.org/10.1098/rspb.1987.0053

Howard, J., & Snyder, A. W. (1983). Transduction as a limitation on compound eye function and design. *Proceedings of the Royal Society of London. Series B. Biological Sciences*, *217*(1208), 287–307. https://doi.org/10.1098/rspb.1983.0011

Juusola, M., Kouvalainen, E., Järvilehto, M., & Weckström, M. (1994). Contrast gain, signal-to-noise ratio, and linearity in light-adapted blowfly photoreceptors. *Journal of General Physiology*, *104*(3), 593–621. https://doi.org/10.1085/jgp.104.3.593

Keister, M., & Buck, J. (1961). Respiration of *Phormia regina* in relation to temperature and oxygen. *Journal of Insect Physiology*, *7*(1), 51–72. https://doi.org/10.1016/0022-1910(61)90044-0

Kelber, A., & Somanathan, H. (2019). Spatial vision and visually guided behavior in Apidae. *Insects*, *10*(12), 418. https://doi.org/10.3390/insects10120418

Kim, J. (2014). Absorption-assisted mode transformation in butterfly compound eyes. *Scientific Reports*, *4*(11), 6291. https://doi.org/10.1038/srep06291

Kirschfeld, K. (1976). The resolution of lens and compound eyes. In F. Zettler & R. Weiler (Eds.), *Neural principles in vision* (pp. 354–370). Springer. https://doi.org/10.1007/978-3-642-66432-8_19

Kröger, R. H., & Biehlmaier, O. (2009). Space-saving advantage of an inverted retina. *Vision Research*, *49*(18), 2318–2321. https://doi.org/10.1016/j.visres.2009.07.001

Labhart, T., & Nilsson, D.-E. (1995). The dorsal eye of the dragonfly Sympetrum: specializations for prey detection against the blue sky. *Journal of Comparative Physiology A*, *176*(4), 437–453. https://doi.org/10.1007/BF00196410

Land, M. F. (1981). Optics and vision in invertebrates. In H. Autrum (Ed.), *Handbook of sensory physiology* (pp. 471–593, Vol. VII/6B). Springer-Verlag.

Land, M. F. (1985). The morphology and optics of spider eyes. In F. G. Barth (Ed.), *Neurobiology of arachnids* (pp. 53–78). Springer. https://doi.org/10.1007/978-3-642-70348-5_4

Land, M. F., & Eckert, H. (1985). Maps of the acute zones of fly eyes. *Journal of Comparative Physiology A*, *156*(4), 525–538. https://doi.org/10.1007/BF00613976

Land, M. F., & Fernald, R. D. (1992). The evolution of eyes. *Annual Review of Neuroscience*, *15*, 1–29. https://doi.org/10.1146/annurev.ne.15.030192.000245

Land, M. F. (1997). Visual acuity in insects. *Annual Review of Entomology*, *42*(1), 147–177. https://doi.org/10.1146/annurev.ento.42.1.147

Laughlin, S. B. (1981). A simple coding procedure enhances a neuron's information capacity. *Zeitschrift fur Naturforschung C*, *36*, 910–912.

Laughlin, S. B., & McGinness, S. (1978). The structures of dorsal and ventral regions of a dragonfly retina. *Cell and Tissue Research*, *188*(3), 427–447.

Laughlin, S. B., van Steveninck, R. R. R., & Anderson, J. C. (1998). The metabolic cost of neural information. *Nature Neuroscience*, *1*(1), 36–41. https://doi.org/10.1038/236

Laughlin, S. B., & Weckström, M. (1993). Fast and slow photoreceptors—a comparative study of the functional diversity of coding and conductances in the Diptera. *Journal of Comparative Physiology A*, *172*(5), 593–609. https://doi.org/10.1007/BF00213682

Menzel, J. G., Wunderer, H., & Stavenga, D. G. (1991). Functional morphology of the divided compound eye of the honeybee drone (*Apis mellifera*). *Tissue and Cell*, *23*(4), 525–535. https://doi.org/10.1016/0040-8166(91)90010-Q

Nijhout, H. F., & Emlen, D. J. (1998). Competition among body parts in the development and evolution of insect morphology. *Proceedings of the National Academy of Sciences*, *95*(7), 3685–3689. https://doi.org/10.1073/pnas.95.7.3685

Nilsson, D.-E. (2013). Eye evolution and its functional basis. *Visual Neuroscience*, *30*(1–2), 5–20. https://doi.org/10.1017/S0952523813000035

Nilsson, D.-E. (2021). The diversity of eyes and vision. *Annual Review of Vision Science*, *7*(1), 19–41. https://doi.org/10.1146/annurev-vision-121820-074736

Nilsson, D.-E., & Land, M. F. (2012). *Animal eyes* (2nd.). Oxford University Press.

Nilsson, D.-E., & Pelger, S. (1994). A pessimistic estimate of the time required for an eye to evolve. *Proceedings of the Royal Society B: Biological Sciences*, *256*(1345), 53–58. https://doi.org/10.1098/rspb.1994.0048

Niven, J. E., Anderson, J. C., & Laughlin, S. B. (2007). Fly photoreceptors demonstrate energy-information trade-offs in neural coding. *PLoS Biology*, *5*(4), 828–840. https://doi.org/10.1371/journal.pbio.0050116

Niven, J. E., & Laughlin, S. B. (2008). Energy limitation as a selective pressure on the evolution of sensory systems. *Journal of Experimental Biology*, *211*(11), 1792–1804. https://doi.org/10.1242/jeb.017574

Niven, J. E., & Scharlemann, J. P. (2005). Do insect metabolic rates at rest and during flight scale with body mass? *Biology Letters*, *1*(3), 346–349. https://doi.org/10.1098/rsbl.2005.0311

Oakley, T. H., & Speiser, D. I. (2015). How complexity originates: The evolution of animal eyes. *Annual Review of Ecology, Evolution, and Systematics*, *46*(1), 237–260. https://doi.org/10.1146/annurev-ecolsys-110512-135907

Okawa, H., Sampath, A. P., Laughlin, S. B., & Fain, G. L. (2008). ATP consumption by mammalian rod photoreceptors in darkness and in light. *Current Biology*, *18*(24), 1917–1921. https://doi.org/10.1016/j.cub.2008.10.029

Pangršič, T., Stušek, P., Belušič, G., & Zupančič, G. (2005). Light dependence of oxygen consumption by blowfly eyes recorded with a magnetic diver balance. *Journal of Comparative Physiology A*, *191*(1), 75–84. https://doi.org/10.1007/s00359-004-0571-y

Perl, C. D., & Niven, J. E. (2016). Differential scaling within an insect compound eye. *Biology Letters*, *12*(3), 20160042. https://doi.org/10.1098/rsbl.2016.0042

Piersma, T., & van Gils, J. A. (2011). *The flexible phenotype*. Oxford University Press.

Provis, J. M., Dubis, A. M., Maddess, T., & Carroll, J. (2013). Adaptation of the central retina for high acuity vision: Cones, the fovea and the avascular zone. *Progress in Retinal and Eye Research*, *35*, 63–81. https://doi.org/10.1016/j.preteyeres.2013.01.005

Rigosi, E., Wiederman, S. D., & O'Carroll, D. C. (2017). Photoreceptor signalling is sufficient to explain the detectability threshold of insect aerial pursuers. *The Journal of Experimental Biology*, *220*(23), 4364–4369. https://doi.org/10.1242/jeb.166207

Rossel, S. (1979). Regional differences in photoreceptor performance in the eye of the praying mantis. *Journal of Comparative Physiology*, *131*(2), 95–112. https://doi.org/10.1007/BF00619070

Ruderman, D. L. (1997). Origins of scaling in natural images. *Vision Research*, *37*(23), 3385–3398. https://doi.org/10.1016/S0042-6989(97)00008-4

Scales, J. A., & Butler, M. A. (2016). The relationship between microhabitat use, allometry and functional variation in the eyes of Hawaiian *Megalagrion* damselflies. *Functional Ecology*, *30*(3), 356–368. https://doi.org/10.1111/1365-2435.12479

Schreiber, S., Machens, C. K., Herz, A. V. M., & Laughlin, S. B. (2002). Energy-efficient coding with discrete stochastic events. *Neural Computation*, *14*(6), 1323–1346. https://doi.org/10.1162/089976602753712963

Seitz, G. (1968). Der Strahlengang in Appositionsauge von *Calliphora erythrocephala* (Meig.) *Zeitschrift fur Vergleichende Physiologie*, *59*(2), 205–231.

Smith, W. C., & Butler, J. F. (1991). Ultrastructure of the Tabanidae compound eye: Unusual features for Diptera. *Journal of Insect Physiology*, *37*(4), 287–296. https://doi.org/10.1016/0022-1910(91)90063-6

Snyder, A. W. (1977). Acuity of compound eyes - physical limitations and design. *Journal of Comparative Physiology*, *116*(2), 161–182. https://doi.org/10.1007/BF00605401

Snyder, A. W. (1979). Physics of vision in compound eyes. In H. Autrum (Ed.), *Handbook of sensory physiology* (pp. 225–313, Vol. VII/6A). Springer.

Snyder, A. W., Bossomaier, T. J., & Hughes, A. (1994). The theory of comparative eye design. In C. Blakemore (Ed.), *Vision: Coding and efficiency* (pp. 45–52). C.U.P.

Snyder, A. W., Stavenga, D. G., & Laughlin, S. B. (1977). Spatial information capacity of compound eyes. *Journal of Comparative Physiology*, *116*(2), 183–207. https://doi.org/10.1016/0042-6989(77)90151-1

Song, Z., & Juusola, M. (2014). Refractory sampling links efficiency and costs of sensory encoding to stimulus statistics. *The Journal of Neuroscience*, *34*(21), 7216–7237. https://doi.org/10.1523/JNEUROSCI.4463-13.2014

Song, Z., Postma, M., Billings, S. A., Coca, D., Hardie, R. C., & Juusola, M. (2012). Stochastic, adaptive sampling of information by microvilli in fly photoreceptors. *Current Biology*, *22*(15), 1371–1380. https://doi.org/10.1016/j.cub.2012.05.047

Stavenga, D. G. (2003a). Angular and spectral sensitivity of fly photoreceptors. I. Integrated facet lens and rhabdomere optics. *Journal of Comparative Physiology A: 189*(1), 1–17. https://doi.org/10.1007/s00359-002-0370-2

Stavenga, D. G. (2003b). Angular and spectral sensitivity of fly photoreceptors. II. Dependence on facet lens F-number and rhabdomere type in *Drosophila*. *Journal of Comparative Physiology A*, *189*(3), 189–202. https://doi.org/10.1007/s00359-003-0390-6

Stavenga, D. G. (2004a). Angular and spectral sensitivity of fly photoreceptors. III. Dependence on the pupil mechanism in the blowfly *Calliphora*. *Journal of Comparative Physiology A: 190*(2), 115–129. https://doi.org/10.1007/s00359-003-0477-0

Stavenga, D. G. (2004b). Visual acuity of fly photoreceptors in natural conditions - dependence on UV sensitizing pigment and light-controlling pupil. *Journal of Experimental Biology*, *207*(10), 1703–1713. https://doi.org/10.1242/jeb.00949

Stavenga, D. G., Kruizinga, R., & Leertouwer, H. (1990). Dioptrics of the facet lenses of male blowflies *Calliphora* and *Chrysomyia*. *Journal of Comparative Physiology A*, *166*(3), 365–371. https://doi.org/10.1007/BF00204809

Stearns, S. C. (1989). Trade-offs in life-history evolution. *Functional Ecology*, *3*(3), 259–268. https://doi.org/10.2307/2389364

Sterling, P., & Laughlin, S. (2015). *Principles of neural design*. MIT Press.

Straw, A. D., Warrant, E. J., & O'Carroll, D. C. (2006). A 'bright zone' in male hoverfly *Eristalis tenax* eyes and associated faster motion detection and increased contrast sensitivity. *Journal of Experimental Biology*, *209*, 4339–4354. https://doi.org/10.1242/jeb.02517

Sumner-Rooney, L. (2018). The kingdom of the blind: Disentangling fundamental drivers in the evolution of eye loss. *Integrative and Comparative Biology*, *58*(3), 372–385. https://doi.org/10.1093/icb/icy047

Sumner-Rooney, L., Kenny, N. J., Ahmed, F., & Williams, S. T. (2019). The utility of micro-computed tomography for the non-destructive study of eye microstructure in snails. *Scientific Reports*, *9*, 15411. https://doi.org/10.1038/s41598-019-51909-z

Tatler, B., O'Carroll, D. C., & Laughlin, S. B. (2000). Temperature and the temporal resolving power of fly photoreceptors. *Journal of Comparative Physiology A*, *186*(4), 399–407. https://doi.org/10.1007/s003590050439

Taylor, C., & Weibel, E. (1981). Design of the mammalian respiratory system. I. problem and strategy. *Respiratory Physiology*, *44*, 1–10.

Taylor, G. K., & Thomas, A. L. R. (2014). *Evolutionary biomechanics: Selection, phylogeny and constraint*. Oxford University Press.

Taylor, G. J., Tichit, P., Schmidt, M. D., Bodey, A. J., Rau, C., & Baird, E. (2019). Bumblebee visual allometry results in locally improved resolution and globally improved sensitivity. *eLife*, *8*, e40613. https://doi.org/10.7554/eLife.40613

Thomas, K. N., Gower, D. J., Bell, R. C., Fujita, M. K., Schott, R. K., & Streicher, J. W. (2020). Eye size and investment in frogs and toads correlate with adult habitat, activity pattern and breeding ecology. *Proceedings of the Royal Society B: Biological Sciences*, *287*(1935), 20201393. https://doi.org/10.1098/rspb.2020.1393

Thomas, R. J., Kelly, D. J., & Goodship, N. M. (2004). Eye design in birds and visual constraints on behavior. *Ornitologia Neotropicana*, *15*((Suppl)), 243–250.

van Hateren, J. H. (1992). Theoretical predictions of spatiotemporal receptive fields of fly LMCs, and experimental validation. *Journal of Comparative Physiology A*, *171*(2), 157–170. https://doi.org/10.1007/BF00188924

van Hateren, J. H., Hardie, R. C., Rudolph, A., Laughlin, S. B., & Stavenga, D. G. (1989). The bright zone, a specialized dorsal eye region in the male blowfly *Chrysomyia megacephala*. *Journal of Comparative Physiology A*, *164*(3), 297–308.

van Hateren, J. H., & Schilstra, C. (1999). Blowfly flight and optic flow. II. head movements during flight. *Journal of Experimental Biology*, *202*(11), 1491–1500.

Varela, F., & Wiitanen, W. (1970). Optics of the compound eye of the honeybee *Apis mellifera*. *Journal of General Physiology*, *55*(3), 336–358. https://doi.org/10.1085/jgp.55.3.336

Walls, G. L. (1942). *The vertebrate eye and its adaptive radiation*. Cranbrook Institute of Science.

Wardill, T. J., Fabian, S. T., Pettigrew, A. C., Stavenga, D. G., Nordström, K., & Gonzalez-Bellido, P. T. (2017). A novel interception strategy in a miniature robber fly with extreme visual acuity. *Current Biology*, *27*(6), 854–859. https://doi.org/10.1016/j.cub.2017.01.050

Wehner, R. (1981). Spatial vision in arthropods. In H. Autrum (Ed.), *Handbook of sensory physiology* (pp. 287–616, Vol. VII/6C). Springer-Verlag.

Weibel, E. (2000). *Symmorphosis: On form and function shaping life*. Harvard University Press.

Wilson, M., Garrard, P., & McGinness, S. (1978). The unit structure of the locust compound eye. *Cell and Tissue Research*, *195*(2), 205–226. https://doi.org/10.1007/BF00236720

Witter, M., & Cuthill, I. (1993). The ecological costs of avian fat storage. *Philosophical Transactions of the Royal Society B-Biological Sciences*, *340*(1291), 73–92. https://doi.org/10.1098/rstb.1993.0050

Wong, F., Knight, B. W., & Dodge, F. A. (1980). Dispersion of latencies in photoreceptors of limulus and the adapting-bump model. *Journal of General Physiology*, *76*(5), 517–537. https://doi.org/10.1085/jgp.76.5.517

Yurkiewicz, W. J., & Smyth, T. (1966). Effects of temperature on oxygen consumption and fuel utilization by the sheep blowfly. *Journal of Insect Physiology*, *12*(4), 403–408. https://doi.org/10.1016/0022-1910(66)90003-5

Zeil, J. (1983). Sexual dimorphism in the visual system of flies: The compound eyes and neural superposition in Bibionidae (Diptera). *Journal of Comparative Physiology A*, *150*(3), 379–393. https://doi.org/10.1007/BF00605027

Zhang, L.-Q., Cottaris, N. P., & Brainard, D. H. (2022). An image reconstruction framework for characterizing initial visual encoding. *eLife*, *11*, e71132. https://doi.org/10.7554/eLife.71132